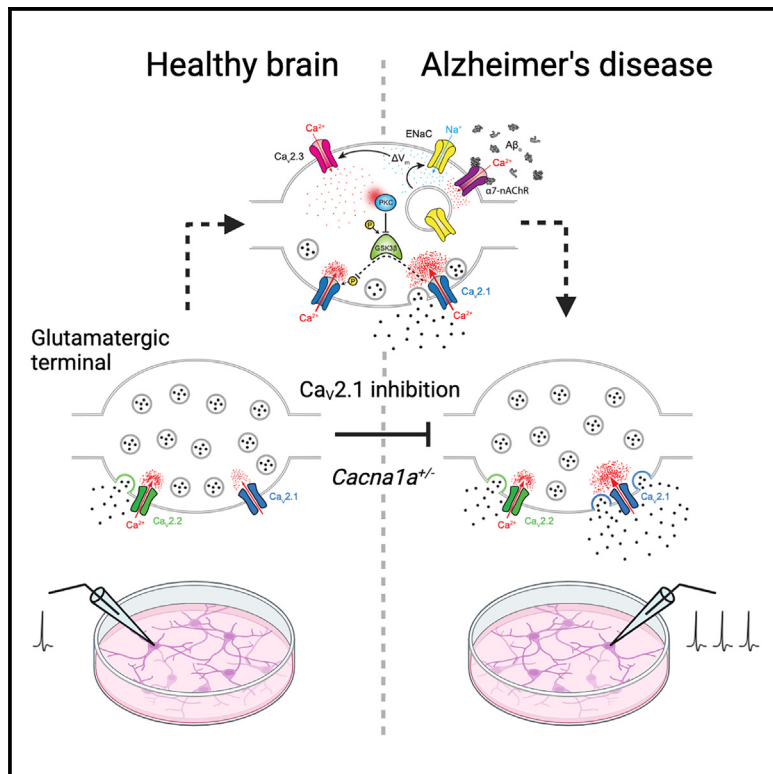


Ca_v2.1 mediates presynaptic dysfunction induced by amyloid β oligomers

Graphical abstract



Authors

Alexander F. Jeans, Zahid Padamsey,
Helen Collins, ..., William L. Klein,
Arn M.J.M. van den Maagdenberg,
Nigel J. Emptage

Correspondence

alexander.jeans@pharm.ox.ac.uk
(A.F.J.),
nigel.emptage@pharm.ox.ac.uk (N.J.E.)

In brief

There is an urgent need for new targets for Alzheimer's disease therapy. Jeans et al. identify a presynaptic signaling pathway engaged by A β oligomers that drives glutamatergic synaptic dysfunction via pathological enhancement of Ca_v2.1 Ca²⁺ channel activity and synaptic vesicle exocytosis. Lowering Ca_v2.1 expression restores normal synaptic function.

Highlights

- A β oligomers drive Ca_v2.1-mediated potentiation of presynaptic exocytosis
- Ca_v2.1 function is upregulated via an ENaC-Ca_v2.3-PKC-GSK-3 β signaling pathway
- Ca_v2.1-mediated potentiation of presynaptic exocytosis is found in AD model mice *in vivo*
- Presynaptic dysfunction can be rescued *in vivo* by lowering Ca_v2.1 expression



Article

Ca_v2.1 mediates presynaptic dysfunction induced by amyloid β oligomers

Alexander F. Jeans,^{1,4,*} Zahid Padamsey,¹ Helen Collins,¹ William Foster,¹ Sally Allison,¹ Steven Diersmeier,¹ William L. Klein,² Arn M.J.M. van den Maagdenberg,³ and Nigel J. Emptage^{1,*}

¹Department of Pharmacology, University of Oxford, Mansfield Road, Oxford OX1 3QT, UK

²Department of Neurobiology and Physiology, Northwestern University, Evanston, IL 60208, USA

³Departments of Human Genetics and Neurology, Leiden University Medical Centre, 2300 RC Leiden, the Netherlands

⁴Lead contact

*Correspondence: alexander.jeans@pharm.ox.ac.uk (A.F.J.), nigel.emptage@pharm.ox.ac.uk (N.J.E.)

<https://doi.org/10.1016/j.celrep.2025.115451>

SUMMARY

Synaptic dysfunction is an early pathological phenotype of Alzheimer's disease (AD) that is initiated by oligomers of amyloid β peptide (A β _os). Treatments aimed at correcting synaptic dysfunction could be beneficial in preventing disease progression, but mechanisms underlying A β _o-induced synaptic defects remain incompletely understood. Here, we uncover an epithelial sodium channel (ENaC) - Ca_v2.3 - protein kinase C (PKC) - glycogen synthase kinase-3 β (GSK-3 β) signal transduction pathway that is engaged by A β _os to enhance presynaptic Ca_v2.1 voltage-gated Ca²⁺ channel activity, resulting in pathological potentiation of action-potential-evoked synaptic vesicle exocytosis. We present evidence that the pathway is active in human APP transgenic mice *in vivo* and in human AD brains, and we show that either pharmacological Ca_v2.1 inhibition or genetic Ca_v2.1 haploinsufficiency is sufficient to restore normal neurotransmitter release. These findings reveal a previously unrecognized mechanism driving synaptic dysfunction in AD and identify multiple potentially tractable therapeutic targets.

INTRODUCTION

Alzheimer's disease (AD) is increasing in prevalence in the aging population, and the identification of effective disease-modifying treatments remains a priority. Numerous lines of evidence suggest that amyloid β (A β) peptides, in particular A β oligomers (A β _os), are a key trigger of the synaptic toxicity and cognitive decline that characterize AD.¹ Exposure to A β _os produces multiple effects on different cell types,² with alterations in synaptic transmission being among the earliest observed. Aberrantly enhanced synaptic activity in excitatory neurons of the cortex and hippocampus is a particularly consistent early finding in both AD model systems and patients,³ although the underlying mechanisms remain a matter of debate.^{4,5}

Since dysregulation of synaptic transmission is considered to be one of the key substrates of early cognitive decline in AD,³ elucidating the underlying mechanisms is of critical importance in order to devise effective new therapies. Accordingly, we set out to understand A β _o-induced alterations in synaptic transmission in a variety of well-characterized AD model systems.

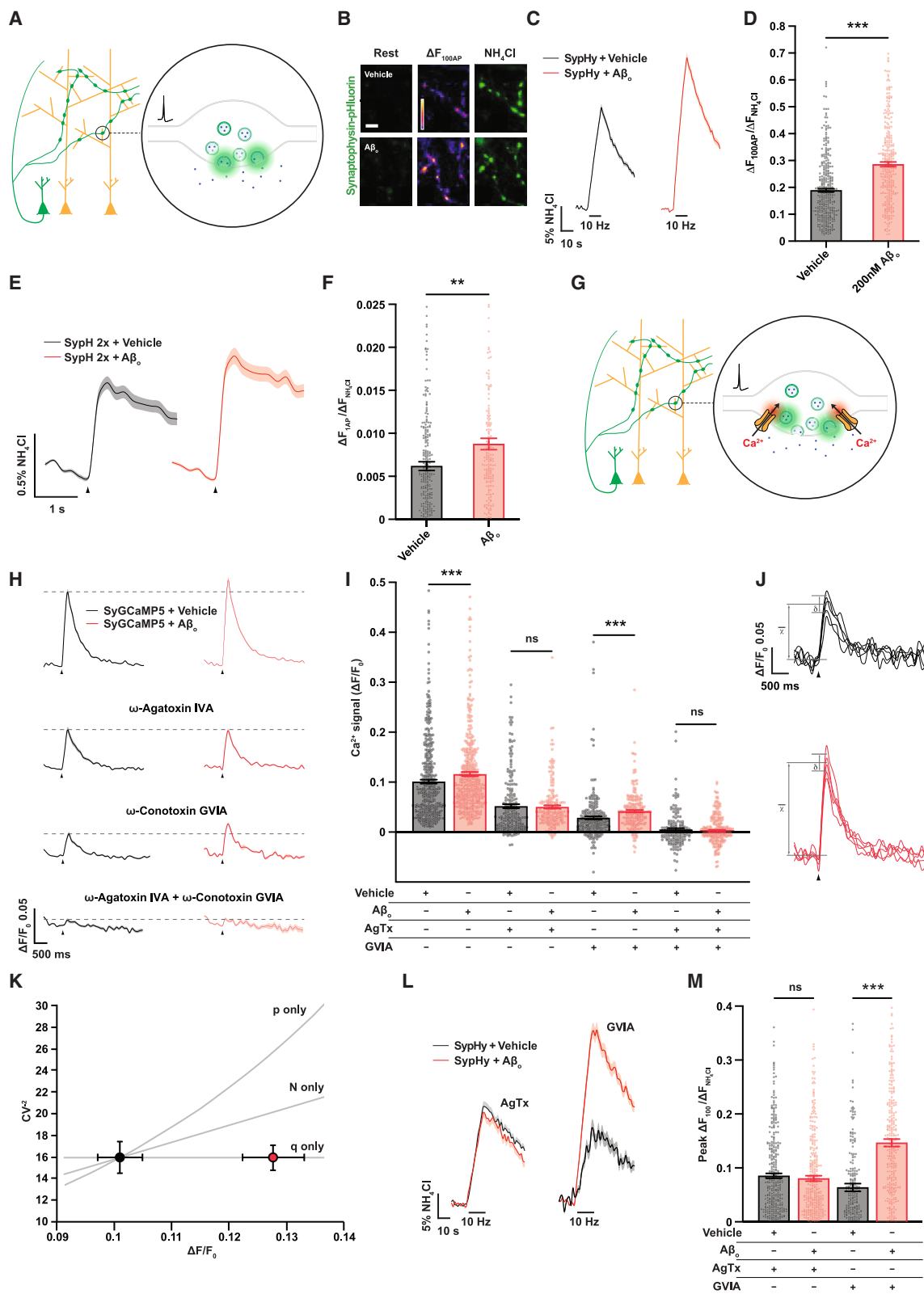
RESULTS

A β _os induce a robust enhancement of evoked synaptic vesicle exocytosis in hippocampal neurons due to increased Ca²⁺ entry through presynaptic Ca_v2.1 channels

We first studied the effects of acute applications of A β _os on synaptic transmission using patch-clamp recordings in cultured rat hippocampal pyramidal neurons. Although oligomers of a variety of sizes have been implicated in A β -mediated synaptotoxicity,⁶ we chose to focus on the effects of a well-characterized, pathologically relevant synthetic preparation of small oligomers of A β ₁₋₄₂ (Figure S1A), which have consistently been identified as the most synaptotoxic A β species and are present in AD-affected brains.^{7,8} Although there is a risk that synthetic oligomers might not replicate the posttranslational modifications of those isolated from native mouse or human brain, multiple studies have demonstrated that, in practice, their properties at both the structural and the pathological level align extremely well with those of their brain-derived counterparts.⁶

A 2 h incubation with 200 nM A β _o induced an increase in overall excitatory glutamatergic synaptic activity, while inhibitory





(legend on next page)

activity was unchanged (Figures S1B–S1D). This could potentially be explained by changes in either the duration or the amplitude of action potentials in excitatory glutamatergic neurons or a change in neuronal excitability. However, we found that none of these parameters were altered by $\text{A}\beta_o$ treatment (Figures S1E–S1I), although we note that these recordings were made at the soma, and it remains formally possible that the voltage waveform at the presynaptic terminal, which is not feasible to record directly, could be different. We then focused on the regulation of neurotransmitter release at the presynaptic terminal, which we imaged in neurons expressing a high-resolution fluorescent reporter of synaptic vesicle exocytosis, synaptophysin-pHluorin (SypHy)⁹ (Figure 1A). Incubation with $\text{A}\beta_o$ s produced a >40% potentiation of exocytosis in response to a 10 Hz stimulus train (Figures 1B–1D), an effect that was similar across a wide range of $\text{A}\beta_o$ concentrations (Figures S2A and S2B). To confirm that this effect does not reflect changes at inhibitory terminals, we expressed a pHluorin fused to the vesicular GABA transporter (vGAT-pHluorin) under the control of the GAD67 promoter, which restricts expression to GABAergic synapses.¹⁰ This showed no change in exocytosis following $\text{A}\beta_o$ incubation (Figures S2C–S2E).

During the repetitive action potential firing elicited by stimulus trains, the total amount of exocytosis at each synapse is regulated by multiple parameters, including the rate of replenishment of the pool of available synaptic vesicles and the probability that

any single action potential will drive the exocytosis of one or more release-competent vesicles, known as the probability of release. Therefore, to refine possible targets of $\text{A}\beta_o$ action, we examined exocytosis in response to single action potential stimuli directly using SypHluorin 2x (SypH 2x), a derivative of SypHy with enhanced sensitivity.¹¹ The average single-stimulus SypH 2x response measured over 10 trials was around 40% greater in neurons exposed to $\text{A}\beta_o$ s, indicating that this treatment robustly enhances probability of release (Figures 1E and 1F).

The probability of neurotransmitter release at hippocampal boutons is set by action-potential-evoked Ca^{2+} influx through presynaptic voltage-gated Ca^{2+} channels (VGCCs).¹² We studied boutonal Ca^{2+} transients using the presynaptically localized Ca^{2+} reporter SyGCaMP5 (Figure 1G). Focusing on single-stimulus-evoked events, since these lie within the linear range of this probe,¹³ we observed an approximately 10% increase in Ca^{2+} influx in the presence of $\text{A}\beta_o$ s (Figures 1H and 1I). We used optical fluctuation analysis, which analyzes trial-to-trial variation in boutonal Ca^{2+} transients to determine whether changes in Ca^{2+} influx are due to changes in the number or properties of VGCCs.¹⁴ This demonstrated that the enhanced presynaptic Ca^{2+} influx was due to an increase in unitary Ca^{2+} channel currents rather than the number of available channels or their opening probability (Figures 1J and 1K). In addition to altered Ca^{2+} influx, changes in probability of release can also be driven by changes in the proximity of VGCCs to the neurotransmitter

Figure 1. $\text{A}\beta$ oligomers induce a robust enhancement of evoked synaptic vesicle exocytosis in hippocampal neurons due to enhanced Ca^{2+} entry through presynaptic $\text{Ca}_{v2.1}$ channels

(A) Imaging neurotransmitter release with a pHluorin probe. Synaptophysin-pHluorin (SypHy) is expressed on the luminal face of synaptic vesicles, where its fluorescence is quenched at intravesicular pH ~5.5. Exocytosis exposes the luminal face of the vesicle to extracellular pH ~7.4, unquenching SypHy fluorescence (green).

(B) Representative images showing hippocampal neuronal boutons expressing SypHy and incubated for 2 h with either 200 nM $\text{A}\beta_o$ or vehicle control. Middle column shows the increase in fluorescence after stimulation at 10 Hz for 10 s. Right-hand side shows maximal signal following unquenching of SypHy with NH_4Cl , used for normalization as a control for SypHy expression level. Scale bar, 5 μm .

(C) Average SypHy fluorescence traces during 10 Hz/10 s stimulation.

(D) Mean peak amplitudes of 10 Hz/10 s responses (control, $n = 364$ synapses from seven coverslips, and 200 nM $\text{A}\beta_o$, $n = 323$ synapses from seven coverslips).

(E) Fluorescence traces showing the mean 10 trial average response of $\text{A}\beta_o$ - or vehicle control-incubated boutons expressing the enhanced sensitivity pHluorin SypH 2x to a single stimulus. Arrow indicates delivery of stimulus.

(F) Mean amplitudes of (10 trial average) responses to a single stimulus (vehicle-treated control, $n = 288$ boutons from eight coverslips, and $\text{A}\beta_o$, $n = 199$ boutons from seven coverslips).

(G) Imaging presynaptic Ca^{2+} entry. The presynaptically targeted Ca^{2+} reporter SyGCaMP5 is a synaptophysin-GCaMP5 fusion protein that is expressed on the outer surface of synaptic vesicles where Ca^{2+} entry (red) via voltage-gated channels causes it to fluoresce (green).

(H) Fluorescence traces showing the mean five trial average response of $\text{A}\beta_o$ - or vehicle control-incubated boutons expressing SyGCaMP5 to a single stimulus, with VGCC-blocking peptides ω -agatoxin IVA ($\text{Ca}_{v2.1}$) and/or ω -conotoxin GVIA ($\text{Ca}_{v2.2}$) present as indicated. Arrow indicates delivery of stimulus.

(I) Mean peak amplitudes of (five trial average) Ca^{2+} signals obtained under the conditions indicated (vehicle, $n = 477$ boutons from twelve coverslips; $\text{A}\beta_o$, $n = 505$ boutons from fourteen coverslips; vehicle + ω -agatoxin IVA, $n = 225$ boutons from five coverslips; $\text{A}\beta_o$ + ω -agatoxin IVA, $n = 207$ boutons from six coverslips; vehicle + ω -conotoxin GVIA, $n = 258$ boutons from six coverslips; $\text{A}\beta_o$ + ω -conotoxin GVIA, $n = 240$ boutons from five coverslips; vehicle + ω -agatoxin IVA + ω -conotoxin GVIA, $n = 170$ boutons from eight coverslips; and $\text{A}\beta_o$ + ω -agatoxin IVA + ω -conotoxin GVIA, $n = 268$ boutons from ten coverslips). ANOVA with *post hoc* t test and Sidak correction.

(J) Optical fluctuation analysis of Ca^{2+} responses using data from vehicle- and $\text{A}\beta_o$ -treated boutons represented in (I). Analysis of trial-to-trial fluctuations in responses enables differences in mean response between groups to be attributed to changes in the number of VGCCs (N), their open probability (p), or their unitary Ca^{2+} currents (q). Representative five trial sets of traces are shown (\bar{x} , mean; δ , standard deviation of $\Delta[\text{Ca}^{2+}]$; arrowheads indicate delivery of stimulus).

(K) Relationship between the mean of the inverse squared coefficient of variation (CV^{-2}) and the mean amplitude of responses in each condition. The gray lines are predictions of what would be observed if the change in Ca^{2+} response amplitude were explained solely by changes in N, p, or q. The Bayesian information criterion (BIC) confirmed that, of the three possible models, variation in q provided the best fit to the experimental data (ΔBIC for both p vs. q and N vs. q > 200 in favor of q).

(L) $\text{Ca}_{v2.1}$ (ω -agatoxin IVA sensitive) but not $\text{Ca}_{v2.2}$ (ω -conotoxin GVIA sensitive) VGCCs are necessary for $\text{A}\beta_o$ -enhanced exocytosis. Average SypHy fluorescence traces obtained in response to 100 stimuli delivered at 10 Hz in the presence of either ω -agatoxin IVA (left) or ω -conotoxin GVIA (right) are shown.

(M) Mean peak amplitudes of responses to 100 stimuli delivered at 10 Hz in ω -agatoxin IVA or ω -conotoxin GVIA (control + agatoxin, $n = 382$ boutons from seven coverslips; $\text{A}\beta_o$ + agatoxin, $n = 372$ boutons from seven coverslips; control + conotoxin, $n = 259$ boutons from seven coverslips; and $\text{A}\beta_o$ + conotoxin, $n = 322$ boutons from seven coverslips).

Shading or error bars represent \pm SEM. ** $p < 0.01$, *** $p < 0.0001$, and ns, non-significant.

release machinery.¹² We tested this using the slow Ca^{2+} chelator EGTA. If the chelator is present in excess, and therefore non-saturable, the percentage inhibition of exocytosis will depend on the distance between the Ca^{2+} channel pore and the release sensor (synaptotagmin), as well as the chelator's Ca^{2+} binding kinetics.¹⁵ Importantly, it will not be sensitive to the total Ca^{2+} influx through the channel,¹⁵ which changes following $\text{A}\beta_o$ exposure. We found that a brief incubation in a set concentration of cell-permeative EGTA-AM (200 μM for 90 s) depressed exocytosis in response to a single stimulus to a lesser extent following $\text{A}\beta_o$ incubation (Figures S2F and S2G), indicating tighter physical coupling of VGCCs to the release machinery. Together, these changes can account fully for the enhancement of synaptic vesicle exocytosis by $\text{A}\beta_o$ s, particularly given the highly non-linear, co-operative relationship between Ca^{2+} influx and vesicular neurotransmitter release at mammalian hippocampal synapses.¹⁶

Ca^{2+} influx at glutamatergic hippocampal terminals is predominantly dependent upon a combination of $\text{Ca}_v2.2$ and $\text{Ca}_v2.1$ VGCCs,¹⁷ and we used the specific Ca^{2+} -channel-blocking peptides ω -conotoxin GVIA ($\text{Ca}_v2.2$) and ω -agatoxin IVA ($\text{Ca}_v2.1$) to dissect the relative contribution of these channels to the $\text{A}\beta_o$ -mediated enhancement of Ca^{2+} entry. We found that the enhancement is abolished only in the presence of ω -agatoxin IVA (Figures 1H and 1I), indicating that it is mediated by $\text{Ca}_v2.1$ but not $\text{Ca}_v2.2$ VGCCs. There was no difference in the Ca^{2+} signal following $\text{A}\beta_o$ incubation when both $\text{Ca}_v2.1$ and $\text{Ca}_v2.2$ were blocked, indicating that non- $\text{Ca}_v2.1/\text{Ca}_v2.2$ Ca^{2+} sources do not contribute significantly (Figures 1H and 1I). To confirm that enhanced Ca^{2+} entry specifically mediated via $\text{Ca}_v2.1$ drives the increase in synaptic vesicle exocytosis, we used VGCC-blocking peptides with SypHy-expressing neurons to show that $\text{Ca}_v2.1$, but not $\text{Ca}_v2.2$, channels are necessary for $\text{A}\beta_o$ -mediated potentiation of the response to a 10 Hz stimulus train (Figures 1L and 1M).

Exocytosis is potentiated via a presynaptic ENaC- $\text{Ca}_v2.3$ -protein kinase C (PKC) signaling axis

We set out to identify the molecular signaling pathway engaged by $\text{A}\beta_o$ s to enhance $\text{Ca}_v2.1$ function and synaptic vesicle exocytosis. We previously reported that a similar specific upregulation of $\text{Ca}_v2.1$ function without change to $\text{Ca}_v2.2$ underlies the potentiation of evoked synaptic vesicle exocytosis in the context of homeostatic synaptic plasticity (HSP),¹⁸ a physiological process that regulates the strength of synapses to maintain activity in neuronal networks within set bounds.¹⁹ Potentiation of synaptic vesicle exocytosis by HSP at both *Drosophila* and mammalian synapses requires the insertion of a preexisting intracellular pool of the epithelial sodium channel (ENaC) into the presynaptic membrane,^{20,21} and we hypothesized that this might be a conserved mechanism for $\text{Ca}_v2.1$ -dependent regulation of presynaptic strength that could also underlie the presynaptic effects of $\text{A}\beta_o$ s. Using immunofluorescence on non-permeabilized and permeabilized neurons in culture to disclose surface and total presynaptic ENaCs, respectively, we found that, while the total presynaptic ENaC level did not change over the time course of the experiments, there was robust insertion of channels into the presynaptic membrane in response to $\text{A}\beta_o$ s (Figures 2A–2C). To then confirm that ENaC activity is necessary

for the ability of $\text{A}\beta_o$ s to enhance exocytosis, we showed that the specific ENaC blocker amiloride²² was able to rescue the effects of $\text{A}\beta_o$ treatment in SypHy-expressing neurons (Figure 2D). In these and subsequent experiments, we chose to assay $\text{Ca}_v2.1$ -driven changes in synaptic vesicle exocytosis rather than examining Ca^{2+} influx directly because the power law relationship between these two parameters¹⁶ lends experimental measurements of exocytosis much greater sensitivity and robustness.

ENaCs carry a Na^+ leak current that causes a modest, chronic depolarization of the bouton.²¹ This could directly augment action-potential-evoked depolarization and thereby Ca^{2+} influx through VGCCs, or, alternatively, ENaCs could enhance $\text{Ca}_v2.1$ function indirectly via recruitment of a signaling pathway. We sought to distinguish between these two possible modes of action by performing a second set of ENaC blockade experiments in which amiloride was not present during the $\text{A}\beta_o$ incubation, allowing potential signaling events downstream of ENaC depolarization to take place, but was applied immediately before stimulation and imaging and stimulation to abolish any direct contribution of ENaC-mediated depolarization to exocytosis. This failed to rescue the effects of $\text{A}\beta_o$ (Figure 2D), suggesting that signaling downstream of channel insertion is necessary. This result is in keeping with the specific enhancement of $\text{Ca}_v2.1$, but not $\text{Ca}_v2.2$, function by ENaC insertion; if direct effects of depolarization on channel function were responsible, a similar enhancement of both VGCC types would be expected, since they have similar gating properties.²³

Chronic, subthreshold depolarization similar to that mediated by ENaCs can initiate intracellular signaling by mobilizing intra- or extracellular Ca^{2+} sources to raise cytoplasmic $[\text{Ca}^{2+}]$. Resting $[\text{Ca}^{2+}]$ was determined at SyGCaMP5-expressing boutons from the GCaMP5 signal,²⁴ and we found that $\text{A}\beta_o$ s elicited a clear $[\text{Ca}^{2+}]$ increase (Figure 2E). We considered possible Ca^{2+} sources that could support this rise, including intracellular stores and presynaptic VGCCs, particularly subtypes with a low activation voltage that are more efficiently opened by subthreshold depolarization, such as Ca_v3 (T-type) or $\text{Ca}_v2.3$ (R-type)²³; we focused on the latter, as Ca_v3 is not expressed at glutamatergic hippocampal terminals.²⁵ We found that incubation with either BAPTA, to chelate extracellular Ca^{2+} , or the $\text{Ca}_v2.3$ -blocking peptide SNX-482 abolished the $\text{A}\beta_o$ -mediated rise in resting cytoplasmic $[\text{Ca}^{2+}]$, indicating that intracellular stores are not sufficient for this, but $\text{Ca}_v2.3$ is required (Figure 2E). We then directly linked $\text{Ca}_v2.3$ to the effects of $\text{A}\beta_o$ s on synaptic vesicle exocytosis by using SypHy-expressing neurons to show that SNX-482 abolishes potentiation of the response to a 10 Hz stimulus train (Figure S2H). Previous work has suggested that $\text{A}\beta_o$ s can activate presynaptic mGluR5 receptors,²⁶ which could potentially also contribute to a rise in cytoplasmic $[\text{Ca}^{2+}]$. We therefore tested the potential involvement of this mechanism, finding that mGluR5 blockade with the specific antagonist SIB-1757 did not prevent the increase in exocytosis seen following $\text{A}\beta_o$ exposure (Figure S2H).

Intracellular Ca^{2+} rises can activate Ca^{2+} -sensing proteins, which in turn can trigger functional changes in a variety of substrates. Aside from the exocytotic Ca^{2+} sensors that mediate excitation-secretion coupling, the predominant Ca^{2+} -sensing proteins expressed presynaptically are PKC²⁷ and calmodulin

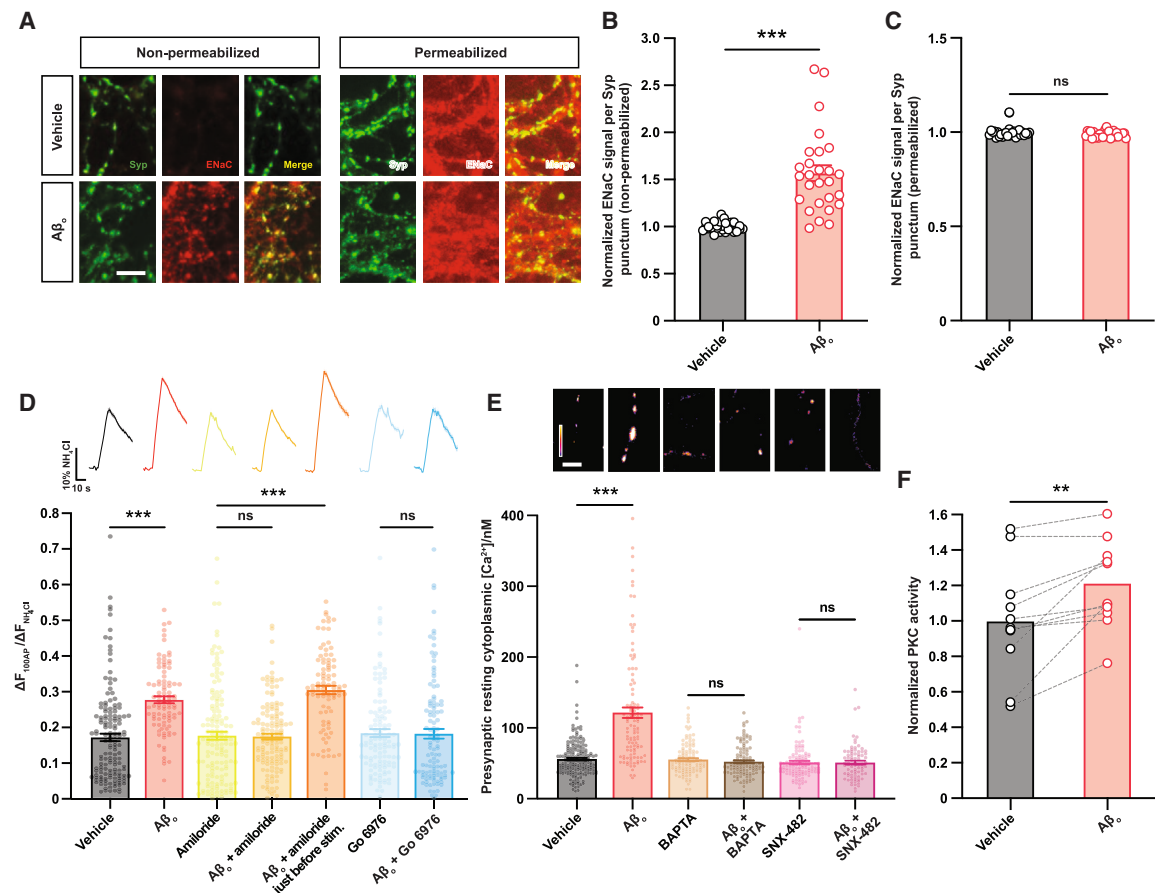


Figure 2. Exocytosis is potentiated via a presynaptic ENaC-Cav2.3-PKC signaling axis

(A) Representative images of ENaC immunofluorescence following treatment as indicated. Labeling of non-permeabilized cells reveals only membrane-inserted surface ENaCs, while permeabilized cells were treated with detergent to ensure that the antibody was able to penetrate the entire cell. To examine presynaptic ENaCs specifically, only labeling overlapping with the presynaptic marker synaptophysin (Syp) was assessed. Scale bar, 5 μm .

(B) Normalized ENaC labeling intensity per synaptophysin-positive punctum in non-permeabilized cells ($n \geq 27$ cells per condition).

(C) Normalized ENaC labeling intensity per synaptophysin-positive punctum in permeabilized cells ($n \geq 28$ cells per condition). Note that these signals were not saturated.

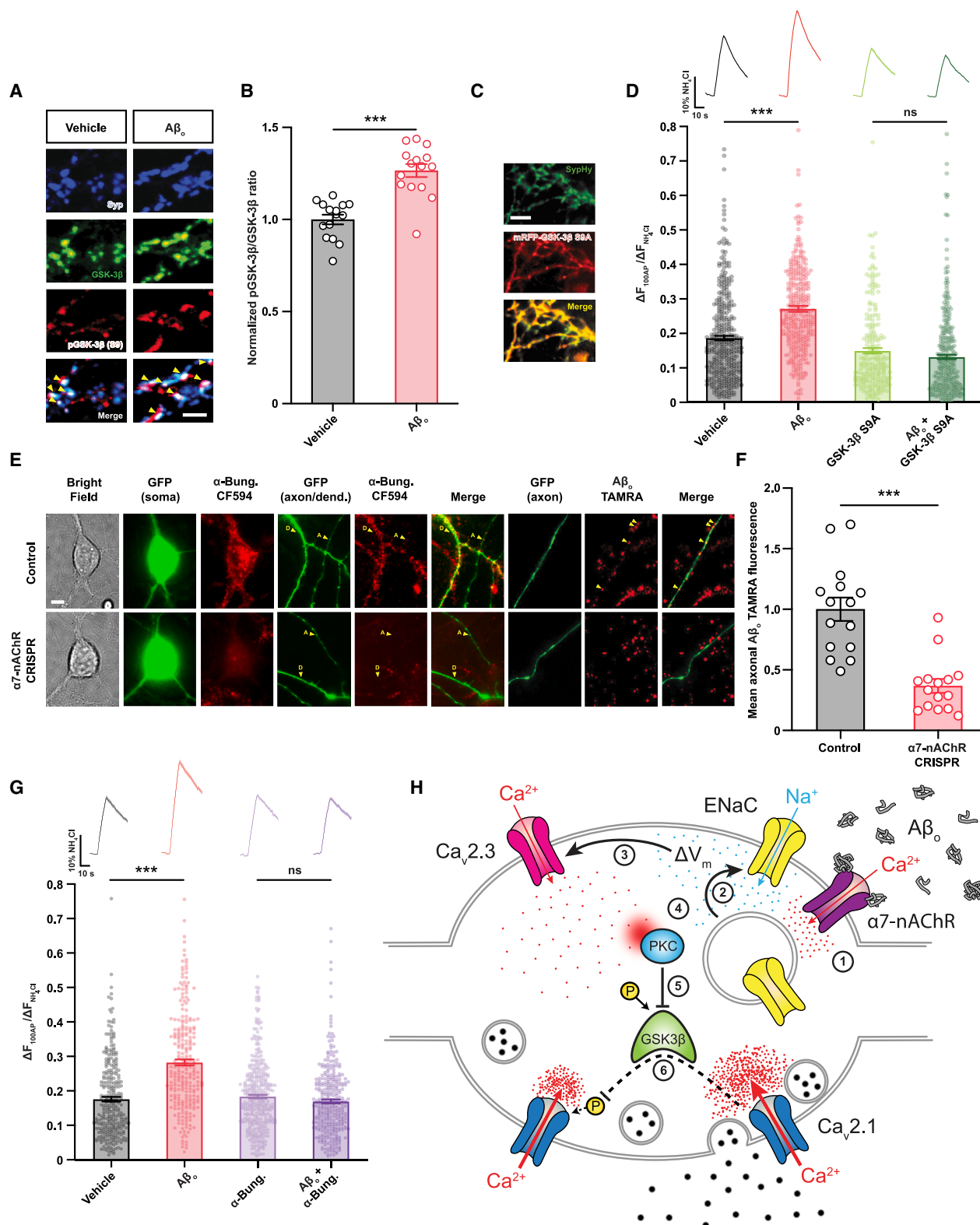
(D) Amiloride, a blocker of the Na^+ leak channel ENaC, and Go 6976, a protein kinase C antagonist, rescue the effect of $\text{A}\beta_o$ s on neurotransmitter release in response to a 100 AP/10 Hz stimulus in SypHy-expressing neuronal cultures. The rescue effect of amiloride is not observed if the drug is applied immediately before stimulation, suggesting that ENaCs regulate $\text{Ca}_v2.1$ via a signaling cascade rather than directly modulating $\text{Ca}_v2.1$ gating via constitutive depolarization, which would require the ENaC to remain open during stimulation. Responses are normalized to maximal NH_4Cl signal, and mean peak amplitudes are shown. Average fluorescence traces are above the bars (vehicle-treated control, $n = 150$ boutons from five coverslips; $\text{A}\beta_o$, $n = 95$ boutons from seven coverslips; amiloride, $n = 150$ boutons from six coverslips; $\text{A}\beta_o + \text{amiloride}$, $n = 146$ boutons from five coverslips; $\text{A}\beta_o + \text{amiloride}$ immediately before stimulation, $n = 90$ boutons from five coverslips; Go 6976, $n = 118$ boutons from five coverslips; and $\text{A}\beta_o + \text{Go 6976}$, $n = 113$ boutons from five coverslips). ANOVA with *post hoc* t test and Sidak correction.

(E) A resting boutonal cytosolic $[\text{Ca}^{2+}]$ rise following $\text{A}\beta_o$ exposure is abolished by either the $\text{Ca}_v2.3$ inhibitor SNX-482 or chelation of extracellular Ca^{2+} with BAPTA. The basal signal from hippocampal neuronal boutons expressing SyCCaMP5 was used along with a maximal signal induced by treatment with the Ca^{2+} ionophore ionomycin to determine resting cytosolic $[\text{Ca}^{2+}]$. Mean values following treatment as indicated are shown (vehicle-treated control, $n = 194$ synapses from six coverslips; $\text{A}\beta_o$, $n = 112$ synapses from six coverslips; BAPTA, $n = 110$ synapses from six coverslips; $\text{A}\beta_o + \text{BAPTA}$, $n = 116$ synapses from six coverslips; SNX-482, $n = 117$ synapses from six coverslips; and $\text{A}\beta_o + \text{SNX-482}$, $n = 81$ synapses from five coverslips). ANOVA with *post hoc* t test and Sidak correction. Image above each bar shows basal SyCCaMP5 signal from a representative field. Scale bar, 5 μm .

(F) Synaptosomes were prepared from individual hippocampal neuronal cultures, then each synaptosome preparation was divided into two and subjected to treatments as indicated. PKC activity was then assessed in synaptosomal lysates using a specific ELISA-based assay ($n = 11$ cultures for all conditions). Paired t test. Shading or error bars represent \pm SEM. ** $p < 0.01$, *** $p < 0.0001$, and ns, non-significant.

(CaM), which directly regulates the activity of a wide variety of proteins, including CaM kinase II, calcineurin, and $\text{Cav}2.1$.²⁸ However, we have shown that $\text{A}\beta_o$ exposure produces a rise in presynaptic cytosolic $[\text{Ca}^{2+}]$ of approximately 60 nM (Fig-

ure 2E), far short of the $[\text{Ca}^{2+}]$ elevation required to activate CaM, which is well into the micromolar range.²⁹ PKC, on the other hand, is activated by nanomolar presynaptic $[\text{Ca}^{2+}]$ rises very comparable to what we have demonstrated.³⁰ To ask



(legend on next page)

whether $\text{A}\beta_o$ s activate presynaptic PKC, we prepared synaptosomes, which comprise the complete presynaptic terminal along with the postsynaptic density, from cultured hippocampal neurons and subjected these to various treatments before assessing PKC activity in synaptosomal lysates with a specific ELISA-based assay. We found that $\text{A}\beta_o$ treatment increased PKC activity in the synaptosomes (Figure 2F), and this effect was blocked by the inclusion of SNX-482 (Figure S2I), corroborating an essential upstream role of $\text{Ca}_V2.3$ in $\text{A}\beta_o$ -linked PKC activation. Finally, to confirm that PKC activity is necessary for the ability of $\text{A}\beta_o$ s to enhance exocytosis, we applied the PKC inhibitor Go 6976 to SypHy-expressing neurons, showing that it rescued the enhancement of synaptic vesicle exocytosis by $\text{A}\beta_o$ s, consistent with an essential role for PKC in this process (Figure 2D). Since resting presynaptic $[\text{Ca}^{2+}]$ varies even among boutons on the same axon,³¹ this mechanism could be consistent with independent regulation of release probability at individual synapses.

GSK-3 β is required for the enhancement of exocytosis by $\text{A}\beta_o$ s

Next, we sought a mechanistic link between PKC activation and enhanced $\text{Ca}_V2.1$ function and exocytosis. Our data show that following exposure to $\text{A}\beta_o$ s, the increase in $\text{Ca}_V2.1$ -driven neurotransmitter release is due to changes in both unitary Ca^{2+} currents and physical coupling of the channels to release machinery. In VGCCs of the Ca_V2 family, both can be achieved via the phosphorylation of a partially conserved intracellular amino acid sequence known as the synprint (synaptic protein interaction) site, which interacts directly with the soluble *N*-ethyl-

maleimide-sensitive factor attachment protein receptor (SNARE) proteins that mediate synaptic vesicle exocytosis.¹² While a number of kinases are known to phosphorylate the $\text{Ca}_V2.2$ synprint site,¹² the $\text{Ca}_V2.1$ synprint sequence is different and just one $\text{Ca}_V2.1$ synprint kinase has been reported to date, glycogen synthase kinase-3 β (GSK-3 β), which phosphorylates $\text{Ca}_V2.1$ to suppress both Ca^{2+} currents and SNARE protein binding.³² It is itself inactivated via phosphorylation at residue serine 9 by a variety of kinases, including PKC.³³ To test its involvement, we first used immunofluorescence to assess the proportion of GSK-3 β within hippocampal presynaptic terminals that is S9 phosphorylated, and therefore inactivated, and found that this increases following $\text{A}\beta_o$ treatment (Figures 3A and 3B). We then co-expressed SypHy together with a constitutively active mutant form of GSK-3 β that is not subject to phosphoregulation at serine 9³⁴ and showed that $\text{A}\beta_o$ s were no longer able to enhance exocytosis (Figures 3C and 3D), indicating that negative phosphoregulation of GSK-3 β is necessary for this effect. To place GSK-3 β in our proposed pathway, we again immunostained $\text{A}\beta_o$ -treated hippocampal neurons for S9-phosphorylated and total GSK-3 β , this time including specific inhibitors of ENaCs, $\text{Ca}_V2.3$, or PKC. As before, we found that $\text{A}\beta_o$ treatment increased the proportion of phospho-GSK-3 β within presynaptic terminals, but that this effect was prevented in the presence of any of the inhibitors (Figure S3A), confirming that GSK-3 β lies mechanistically downstream of each of them. Finally, we considered the question of whether an opposing phosphatase acts alongside GSK-3 β in the regulation of $\text{Ca}_V2.1$ by $\text{A}\beta_o$ s. Very little is known about $\text{Ca}_V2.1$ phosphatases, but it has been shown that the synprint site of the related $\text{Ca}_V2.2$ is dephosphorylated by

Figure 3. Potentiation of exocytosis by $\text{A}\beta_o$ s requires GSK-3 β and $\alpha 7$ -nAChR

(A) Representative fields showing immunofluorescence for total GSK-3 β and GSK-3 β that has been inactivated by phosphorylation of the serine 9 residue. To examine presynaptic GSK-3 β specifically, labeling overlapping with synaptophysin (Syp) was assessed. Bottom shows merged images in which areas of overlapping signal from all three channels appear white (arrowheads). Scale bar, 5 μm .

(B) The fraction of GSK-3 β that has undergone inactivating phosphorylation at S9 is represented as the S9 phosphorylated:total GSK-3 β signal intensity ratio normalized to control average ($n = 15$ fields from five cultures per condition).

(C) mRFP-GSK-3 β (S9A), a constitutively active form of the enzyme insensitive to negative regulatory phosphorylation, was expressed in neurons along with SypHy to probe the requirement for negative regulation of GSK-3 β in $\text{A}\beta_o$ -enhanced synaptic vesicle exocytosis. Representative fields illustrating co-localized signals from SypHy and RFP are shown (scale bar, 5 μm).

(D) Mean peak amplitudes of responses to a 10 Hz/10 s stimulus normalized to maximal NH_4Cl response. Expression of constitutively active GSK-3 β (S9A) reduces the peak exocytotic response in vehicle-treated cultures and abolishes the effect of $\text{A}\beta_o$ s. Average fluorescence traces above bars (control, $n = 412$ boutons from six coverslips; $\text{A}\beta_o$, $n = 374$ boutons from seven coverslips; mRFP-GSK-3 β S9A, $n = 230$ boutons from seven coverslips; and mRFP-GSK-3 β S9A + $\text{A}\beta_o$, $n = 349$ boutons from seven coverslips). ANOVA with *post hoc* t test and Sidak correction.

(E) Representative images showing hippocampal neurons expressing CRISPR-Cas9 knockout constructs targeting either the $\alpha 7$ subunit of nAChR or firefly luciferase as a negative control. Both constructs also include a GFP marker. Images left to right show different views of labeled neurons incubated with either the fluorescently tagged high-affinity $\alpha 7$ -nAChR ligand α -bungarotoxin CF594, demonstrating the loss of surface protein in soma, dendrites (D), and axons (A) of cells expressing the $\alpha 7$ -nAChR CRISPR construct, or $\text{A}\beta_o$ s tagged with the fluorophore tetramethyl rhodamine (TAMRA), showing punctate binding to morphologically identified axons (arrowheads) in control cells that is lost in $\alpha 7$ -nAChR-knockout axons. Scale bar, 10 μm .

(F) Normalized mean axonal fluorescence intensity in control and $\alpha 7$ -nAChR-knockout neurons incubated with $\text{A}\beta_o$ TAMRA ($n = 15$ neurons for both conditions).

(G) The $\alpha 7$ -nAChR antagonist α -bungarotoxin rescues $\text{A}\beta_o$ -induced enhancement of synaptic vesicle exocytosis. Mean peak amplitudes of SypHy responses to a 100 AP/10 Hz stimulus train following the indicated treatments, with average traces above bars (vehicle-treated control, $n = 324$ synapses from seven coverslips; $\text{A}\beta_o$, $n = 273$ synapses from seven coverslips; vehicle + α -bungarotoxin, $n = 392$ boutons from seven coverslips; and $\text{A}\beta_o$ + α -bungarotoxin, $n = 346$ boutons from seven coverslips).

(H) Mechanistic model for enhancement of neurotransmitter release by $\text{A}\beta_o$ s. Arrows and blunted lines indicate activating and inhibitory processes, respectively, and a dashed line indicates inhibition by $\text{A}\beta_o$ s. Our data support a model in which pathological $\text{A}\beta_o$ s elicit presynaptic Ca^{2+} entry via $\alpha 7$ -nAChR (1) to drive insertion of an intracellular pool of ENaCs into the presynaptic membrane (2). This causes an increase in Na^+ influx and a resulting change in presynaptic resting membrane potential ΔV_m , which enhances $\text{Ca}_V2.3$ VGCC opening to elevate resting $[\text{Ca}^{2+}]$ at the presynaptic terminal (3). This $[\text{Ca}^{2+}]$ increase activates protein kinase C (PKC) (4), a negative regulator of GSK-3 β , increasing the fraction of phosphorylated, inactive GSK-3 β (5) and thereby inhibiting GSK-3 β -mediated negative regulation of $\text{Ca}_V2.1$ function (6). The result is increased Ca^{2+} influx via $\text{Ca}_V2.1$ channels, with enhancement of evoked neurotransmitter release. Shading or error bars represent \pm SEM. *** $p < 0.0001$ and ns, non-significant.

multiple phosphatases, including the canonical cellular phosphatases PP1 and PP2a.³⁵ We therefore undertook a preliminary investigation of their involvement in this pathway using a pharmacological inhibitor of PP1 and PP2a, tautomycin. We found that tautomycin alone resulted in a small but significant reduction in exocytosis in SypHy-expressing neurons, while A β _os and tautomycin together restored exocytosis to approximately control levels (Figure S3B). This would be consistent with a scheme in which Ca γ 2.1 function is regulated by a tonic cycle of phosphorylation and dephosphorylation, with A β _os and tautomycin acting to inhibit the relevant kinase and phosphatase, respectively. However, alternative interpretations are also possible, and further study will be required to establish the identity of the Ca γ 2.1 phosphatase beyond doubt.

A β _os bind presynaptic α 7-nAChR to drive ENaC membrane insertion and potentiate exocytosis

To complete the pathway linking A β _os to Ca γ 2.1, we sought to connect A β _os to the mobilization and membrane insertion of ENaCs, a process that is generally poorly understood, although it is known to be Ca $^{2+}$ dependent.³⁶ While the Ca $^{2+}$ source driving ENaC insertion in neurons is not known, nicotinic acetylcholine receptors containing the Ca $^{2+}$ -permeable α 7 subunit (α 7-nAChRs) are strong candidates, since they have been reported to bind A β peptides with picomolar affinity and are expressed on hippocampal presynaptic boutons, where they can be directly activated by A β _os to produce a Ca $^{2+}$ rise.³⁷ To study the binding of A β _os to presynaptic α 7-nAChR, we used CRISPR-Cas9 gene editing to knock out α 7-nAChR expression in cultured hippocampal neurons, confirming the efficacy of the CRISPR-Cas9 construct in abolishing expression of the protein at the cell surface with a fluorescently tagged high-affinity ligand, α -bungarotoxin CF594 (Figure 3E). We showed that axons and boutons of neurons lacking surface α 7-nAChR bound significantly fewer A β _os conjugated with the fluorophore tetramethyl rhodamine (TAMRA) (Figures 3E and 3F), a tag that has previously been shown to have no effect on the proportions of different A β assembly states present in A β _o preparations made according to our protocol.³⁸ Knockout of α 7-nAChR did not significantly alter the postsynaptic/dendritic binding of A β _os (Figure S3C), suggesting that their predominant postsynaptic binding partners are likely to be proteins other than α 7-nAChR. We then used immunofluorescence to show that α -bungarotoxin treatment of A β _o-incubated neurons prevents the insertion of ENaCs into the presynaptic cell membrane (Figure S3D), confirming that A β _o-mediated activation of α 7-nAChR lies mechanistically upstream of ENaC recruitment. We also used α -bungarotoxin to test whether α 7-nAChR function is necessary for the ability of A β _os to enhance exocytosis and found that, while α -bungarotoxin treatment alone did not alter exocytosis in response to a 10 Hz stimulus train, it completely prevented the effects of A β _os (Figure 3G). Thus, an initial nAChR-mediated Ca $^{2+}$ rise can be converted, via the recruitment of ENaCs, to a chronic, depolarization-driven cytoplasmic [Ca $^{2+}$] elevation that ensures efficient activation of the Ca $^{2+}$ sensor in order to sustain a chronic effect on exocytosis.

Together, our data support a model of presynaptic A β _o signaling that functions as follows. A β _os elicit presynaptic Ca $^{2+}$ entry via α 7-nAChR to drive the insertion of an intracellular

pool of ENaCs into the presynaptic membrane. ENaCs mediate a chronic depolarization that, by activating Ca γ 2.3, elevates basal cytoplasmic [Ca $^{2+}$], in turn activating PKC. This kinase then phosphorylates and inactivates the negative Ca γ 2.1 regulator GSK-3 β , thereby potentiating Ca γ 2.1 function and neurotransmitter release (Figure 3H).

Probability of release is enhanced in a Ca γ 2.1-dependent manner at CA3-CA1 synapses in A β _o-treated hippocampal slices

To support the pathophysiological relevance of these neuronal culture-based findings, we wished to explore a potential role for Ca γ 2.1 activity in AD-associated synaptic phenotypes in a more intact setting. We turned initially to electrophysiological recordings in A β _o-incubated acute (*ex vivo*) hippocampal slices from 7- to 8-week-old mice (Figure 4A). We used 10 nM A β _o for these experiments, which has an essentially identical effect to the higher concentration used in culture work (Figures S2A and S2B). The paired-pulse ratio (PPR), which is the ratio of response amplitudes to each of a pair of closely spaced stimuli, is an electrophysiological index of the probability of release.³⁹ We first assessed PPR at CA3-CA1 (Schaffer collateral) synapses and found no apparent effect of A β _o incubation (Figure S4A). However, A β _os have been shown to enhance basal desensitization of synaptic α -amino-3-hydroxy-5-methyl-4-isoxazolepropionic acid receptors (AMPAR),⁴⁰ and changes in AMPAR desensitization can profoundly affect measurements of synaptic transmission, and in particular PPR, at CA3-CA1 synapses.⁴⁰⁻⁴² Therefore, to understand whether AMPAR desensitization influences measurements of PPR in the presence of A β _os, we added the AMPAR desensitization inhibitor cyclothiazide while recording from slices either with or without A β _os in the perfusing ACSF. We found that, while the drug caused a slight enhancement in excitatory postsynaptic potential (EPSP) and a significant increase in PPR in control slices, there was a greater enhancement in EPSP but no change in PPR in A β _o-perfused slices (Figures 4B and 4C). These observations would be in keeping with a role for AMPAR desensitization in PPR under control conditions, limiting the size of the response to the second pulse relative to the first as suggested by previous work.⁴¹ Following exposure to A β _os, however, our data suggest that basal desensitization is enhanced, essentially abolishing this effect.

We used cyclothiazide to study the effect of A β _os on PPR free of desensitization-related confounds. We found that, under these conditions, exposure to A β _os did result in a significant reduction in PPR, indicating an enhanced release probability (Figure S4B). Consistent with this, we have previously shown a similar effect of A β _os in hippocampal slices using direct presynaptic imaging.⁴³ We then asked whether this effect was dependent upon Ca γ 2.1. In the presence of cyclothiazide, CA3-CA1 field EPSPs were enhanced and PPR was again diminished by the addition of A β _os, and these effects were robustly prevented by Ca γ 2.1 blockade with ω -agatoxin IVA (Figures 4D and 4E).

To explore A β -mediated alterations in synaptic function *in vivo*, we used an established and well-characterized model mouse line, J20, which carries a human APP (hAPP) transgene bearing two pathogenic mutations.⁴⁴ We first sought to confirm whether hippocampal neurons in 4- to 8-month-old hAPP transgenic

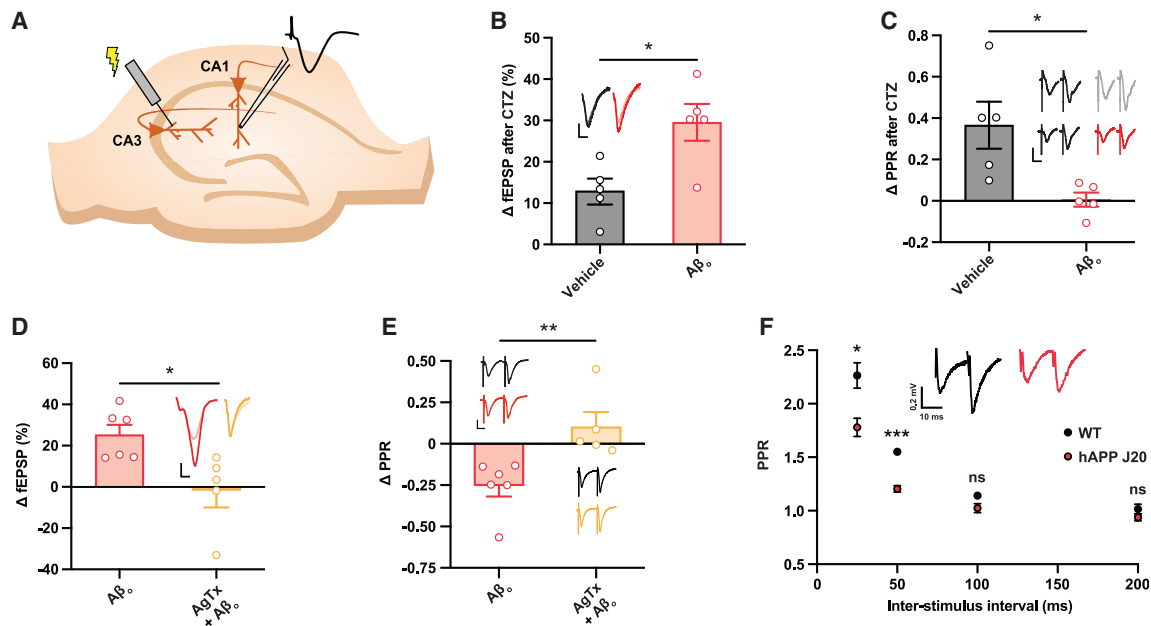


Figure 4. Probability of release is enhanced in a $CaV2.1$ -dependent manner at CA3-CA1 synapses in $A\beta_o$ -treated hippocampal slices

(A) Schematic showing experimental setup for recording of field EPSPs evoked in CA1 of acute hippocampal slices by stimulation of the Schaffer collateral (CA3-CA1) pathway.

(B) Acute hippocampal slices were perfused with buffer containing vehicle or $A\beta_o$ s, and stable basal synaptic transmission was recorded from CA1 for at least 10 min before addition of cyclothiazide (CTZ; 100 μ M). Graph shows the percentage change in field EPSP (fEPSP) 10 min after CTZ addition (vehicle, $n = 5$ slices from two mice, and $A\beta_o$, $n = 5$ slices from three mice). Inset shows sample traces before (faint lines) and after (bold lines) CTZ addition. Scale bars, 0.5 mV and 5 ms.

(C) Change in paired-pulse ratio (PPR) measured in acute slices described in (B). Sample traces are responses before (black) and after (gray/red) addition of CTZ. Scale bars, 1 mV and 5 ms.

(D) Stable recordings were established from acute hippocampal slices perfused with buffer containing CTZ, to prevent $A\beta_o$ -induced AMPAR desensitization, either with or without ω -agatoxin IVA. Graph shows the percentage change in fEPSP 30 min after addition of $A\beta_o$ s (10 nM) ($A\beta_o$, $n = 6$ slices from six mice, and $A\beta_o + \omega$ -agatoxin IVA, $n = 5$ slices from five mice). Inset shows sample traces before (faint lines) and after (bold lines) $A\beta_o$ addition. Scale bars, 0.5 mV and 5 ms.

(E) Change in PPR measured in acute slices described in (D). Sample traces are responses before (black) and 30 min after (red/yellow) addition of $A\beta_o$ s. Scale bars, 1 mV and 5 ms.

(F) PPR at CA3-CA1 synapses assessed at various interstimulus intervals in acute hippocampal slices from 4- to 8-month-old hAPP J20 and littermate wild-type control mice. CTZ was again added to prevent $A\beta_o$ -induced AMPAR desensitization (wild type and hAPP both $n = 6$ slices from three mice). Representative traces show responses at 50 ms intervals. Scale bars, 0.2 mV and 10 ms.

Two-way ANOVA with post hoc t test and Sidak correction. Error bars represent \pm SEM. * $p < 0.05$, ** $p < 0.01$, *** $p < 0.0001$, and ns, non-significant.

mice show evidence of elevated neurotransmitter release by measuring PPR at CA3-CA1 synapses in acute hippocampal slices, this time using a variety of interpulse intervals to increase the sensitivity of the study. As previously, we included cyclothiazide in these experiments to prevent confounding effects due to AMPA receptor desensitization. We found that PPR at 25 and 50 ms intervals was significantly reduced in hAPP mice compared to wild-type littermate controls, indicating enhanced probability of release (Figure 4F).

$CaV2.1$ -dependent enhancement of synaptic vesicle exocytosis at CA3-CA1 synapses in hAPP J20 mice

To further circumvent any potential confounding effects of post-synaptic changes that could influence our measurements, we used the styryl dye FM 1-43 to image synaptic vesicle exocytosis directly in native hippocampal tissue.⁴⁵ Acute hippocampal slices were prepared from 4- to 8-month-old hAPP transgenic mice, and CA3 axons were stimulated while the dye was applied to CA1 to label the total recycling pool of synaptic vesicles (Figure 5A).

Figure 5A). A subsequent 5 Hz stimulus train revealed significantly faster dye unloading in hAPP vs. littermate control slices (Figures 5B and 5C). These results corroborate the electrophysiological data indicating enhanced neurotransmitter release in hAPP transgenic mice. To gain insight into the mechanism underlying enhanced release in hAPP transgenic mouse slices, we crossed the J20 line with transgenic mice bearing a heterozygous deletion of the gene encoding the pore-forming $\alpha 1$ subunit of $CaV2.1$ VGCC ($Cacna1a^{+/-}$).⁴⁶ While homozygous $Cacna1a$ ablation results in severe ataxia, seizures, and premature mortality,⁴⁶ mice carrying a heterozygous deletion lack any readily apparent phenotype.⁴⁷ However, synaptic transmission in $Cacna1a^{+/-}$ slices shows a reduced dependence on $CaV2.1$ (Figure S4C), and we therefore hypothesized that if enhanced $CaV2.1$ activity mediates the effects of $A\beta_o$ s on neurotransmitter release, these effects would be ameliorated by the $Cacna1a^{+/-}$ genotype. We first excluded a background effect of the $Cacna1a^{+/-}$ genotype by confirming that FM dye unloading is not significantly different from that seen at wild-type synapses

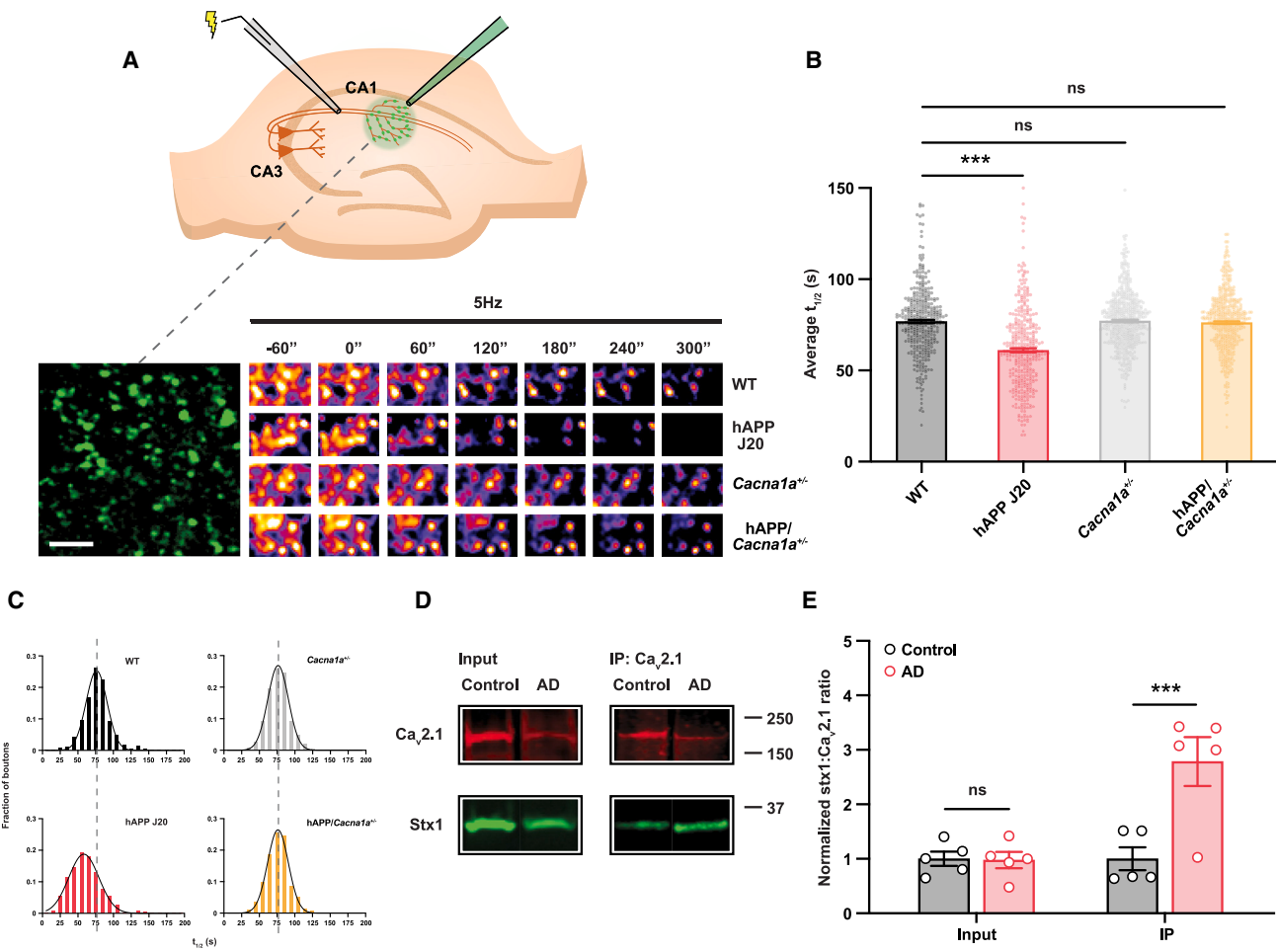


Figure 5. Ca_v2.1-dependent enhancement of synaptic vesicle exocytosis at CA3-CA1 synapses in hAPP J20 mice

(A) Schematic illustrating experimental protocol for visualizing synaptic vesicle exocytosis at CA3-CA1 synapses with FM 1-43 dye. Electrical stimulation of CA3 axons (10 Hz/120 s) turns over the total recycling pool of synaptic vesicles while the dye is applied to CA1, where it is taken up by vesicles as they are endocytosed. After washing to remove bound extracellular FM 1-43, the same axons are stimulated at 5 Hz to unload the dye. Bottom left is a representative field of dye-labeled presynaptic terminals in CA1 from wild-type hippocampus. Bottom right: sample time-lapse images demonstrating stimulus-driven dye loss at synaptic puncta in different mouse genotypes as indicated. Scale bar (applies to all images), 5 μ m.

(B) Average half-life ($t_{1/2}$) of fluorescence unloading for individual puncta fitted with first-order exponential decay functions (wild type, $n = 394$ puncta from five slices; hAPP, $n = 401$ puncta from five slices; *Cacna1a*^{+/−}, $n = 542$ puncta from six slices; and hAPP/*Cacna1a*^{+/−}, $n = 557$ puncta from six slices). ANOVA with *post hoc* t test and Dunnett's correction.

(C) Relative frequency distribution histograms of $t_{1/2}$ for each genotype with superimposed fitted Gaussian distribution (black line). Dashed lines represent mean $t_{1/2}$ for wild-type slices.

(D) The Ca_v2.1 α_1 subunit was immunoprecipitated from purified synaptosomal membrane fractions prepared from the frontal cortex (Brodmann area 9) of AD patients and age-matched controls. Following SDS-PAGE separation, samples were probed with Ca_v2.1 and syntaxin 1 (Stx1) antibodies as indicated. Representative immunoblot bands from both input samples and immunoprecipitates are shown.

(E) Raw immunoblot Stx1:Ca_v2.1 signal ratios from each individual were normalized to the control group mean. Enhanced Stx1:Ca_v2.1 ratio in immunoprecipitated samples indicates stronger interaction between Ca_v2.1 and syntaxin 1 in the brains of AD patients (both groups $n = 5$). Repeated measures ANOVA with *post hoc* t test and Sidak correction.

Error bars represent \pm SEM. *** $p < 0.0001$ and ns, non-significant.

(Figures 5B and 5C). We then showed that the partial genetic suppression of Ca_v2.1 was sufficient to normalize neurotransmitter release at hAPP synapses (Figures 5B and 5C), consistent with a critical mechanistic role for Ca_v2.1 in the enhancement of release in AD model mice *in vivo*. To support the relevance of these experiments to the earlier acute slice work, we also confirmed that the *Cacna1a*^{+/−} genotype conferred resistance

to the effects of A β_0 incubation on presynaptic function as measured using PPR (Figure S4D).

Evidence of enhanced Ca_v2.1 function in hAPP mouse and human AD brains

Finally, we asked whether Ca_v2.1 function is enhanced in human AD brains. Because it is not possible to assess this directly in

postmortem material, we instead took advantage of an indirect index of $\text{Ca}_{\text{v}}2.1$ activation, namely the tighter physical coupling of $\text{Ca}_{\text{v}}2.1$ to the neurotransmitter release machinery that is part of the upregulation of $\text{Ca}_{\text{v}}2.1$ function by $\text{A}\beta_{\text{o}}$ s (Figures S2F and S2G) and of $\text{Ca}_{\text{v}}2.1$ regulation by GSK-3 β more generally.³² The strength of $\text{Ca}_{\text{v}}2.1$ binding to syntaxin 1, a SNARE protein that mediates vesicular neurotransmitter release, provides a measure of this coupling that can be assessed by co-immunoprecipitation. Accordingly, $\text{Ca}_{\text{v}}2.1$ was immunoprecipitated from cortical synaptosomal membrane samples prepared from a cohort of AD patients and non-demented control subjects (Table S1). Immunoprecipitates were subjected to electrophoresis and western blotting with antibodies against $\text{Ca}_{\text{v}}2.1$ and syntaxin 1. This showed that $\text{Ca}_{\text{v}}2.1$ binds more syntaxin 1 in AD brains than in those of control subjects (Figures 5D and 5E), indicating a stronger $\text{Ca}_{\text{v}}2.1$ -SNARE association. We corroborated this observation in aged hAPP mice, supporting their relevance to human disease (Figures S5A and S5B). We noted incidentally that our western blots showed an apparent global reduction in the expression of presynaptic proteins in AD patients (Figure 5D), which was expected, since extensive loss of presynaptic terminals is a feature of advanced AD.⁴⁸

DISCUSSION

Dysregulation of synaptic transmission is an early and critical pathogenic event in AD. While plentiful evidence implicates small oligomers of the $\text{A}\beta$ peptide in a causal role, the underlying mechanisms remain only partially understood. Here, we show that $\text{A}\beta_{\text{o}}$ s engage a presynaptic ENaC - $\text{Ca}_{\text{v}}2.3$ - PKC - GSK-3 β signal transduction pathway that specifically enhances presynaptic $\text{Ca}_{\text{v}}2.1$ VGCC activity, potentiating action-potential-evoked synaptic vesicle exocytosis. We find evidence that the pathway is active in hAPP transgenic mouse models *in vivo* and human AD brains and demonstrate that either pharmacological $\text{Ca}_{\text{v}}2.1$ inhibition or genetic $\text{Ca}_{\text{v}}2.1$ haploinsufficiency is sufficient to normalize neurotransmitter release. These findings reveal a previously unrecognized mechanism driving synaptic dysfunction in AD and identify a number of potentially tractable targets for future therapeutic approaches aimed at the restoration of normal synaptic function. In addition, our data indicate that this mechanism drives excitatory neuronal hyperactivity in hippocampal neuronal networks in culture and is therefore likely, alongside other mechanisms previously described,^{4,5} to contribute to aberrantly enhanced corticohippocampal excitatory activity *in vivo*. While synaptic loss is the major substrate of late-stage cognitive decline in AD,¹ aberrant network-level activity is thought to play a key role much earlier in the disease process.^{3,49} Therapeutic correction of presynaptic functional deficits might, therefore, show benefit from even prodromal stages of AD.

While postsynaptic deficits, such as impairment of synaptic plasticity, have long been recognized as a critical component of $\text{A}\beta_{\text{o}}$ -induced synaptic dysfunction and therefore cognitive decline,¹ presynaptic deficits may be as significant. Indeed, it is well established that perturbations in neurotransmitter release are an important substrate of cognitive changes in a wide variety of neurological disorders.⁵⁰ However, the relatively small body of existing work on presynaptic effects of $\text{A}\beta_{\text{o}}$ demonstrates a striking

diversity of sometimes contradictory effects and mechanisms.^{8,26,51-54} While it is certainly possible that $\text{A}\beta_{\text{o}}$ exhibits pleiotropic actions at the presynaptic terminal, it may also be significant that these effects are reported in a wide range of largely *in vitro* experimental systems, with many studies reliant on a single one. Our study initially exploited the superior experimental and optical access of neuronal cultures to identify an effect as well as to gain detailed insight into the underlying mechanisms. However, an equally important aim was then to support both the effect and the key elements of the mechanism with data from more intact, pathophysiological relevant systems, including hAPP transgenic mice and human tissue, which enhances confidence in our conclusions.

Another cornerstone of our approach was to use, where possible, high-resolution optical methodologies to assess presynaptic neurotransmitter release directly, rather than relying on indirect approaches such as electrophysiology. Not only does this avoid a variety of potential experimental confounds,⁴⁵ here, it helped to uncover an important issue affecting the use of electrophysiological recordings of the PPR to evaluate neurotransmitter release probability. In the physiological context, PPR in part reflects AMPA receptor desensitization that is induced by the first of the paired stimuli, and without this it is artificially increased^{41,42}; our data appear to confirm this. However, in the presence of pathophysiological relevant concentrations of $\text{A}\beta_{\text{o}}$ s, our data suggest that AMPA receptors are constitutively fully desensitized, so that first pulse-induced desensitization cannot take place. The result is an artificial increase in PPR in the presence of $\text{A}\beta_{\text{o}}$ s, giving a falsely low estimate of release probability.³⁹ Accordingly, use of the AMPA receptor desensitization inhibitor cyclothiazide can unmask the effect of $\text{A}\beta_{\text{o}}$ s on PPR, which is otherwise hidden. PPR has been widely used within the AD field for many years, very often to exclude $\text{A}\beta$ -induced presynaptic effects.^{5,8,40,55} However, PPR data obtained in the presence of elevated concentrations of $\text{A}\beta$ should be interpreted with this critical issue borne in mind.

The specific signaling pathway that we identify linking $\text{A}\beta_{\text{o}}$ s to enhanced $\text{Ca}_{\text{v}}2.1$ activity places some components in novel or non-canonical functional roles. While *in vivo* regulation of $\text{Ca}_{\text{v}}2.1$ by a variety of presynaptic interactors, including CaM, G-protein-coupled receptors, and SNAREs, is well recognized,¹² regulation via GSK-3 β -mediated phosphorylation of the synprint site has only been described as a consequence of non-physiological manipulations *in vitro*³² and has not previously been implicated in a specific physiological or pathological pathway. Here, we begin to fill this knowledge gap by demonstrating a role for GSK-3 β regulation of $\text{Ca}_{\text{v}}2.1$ in $\text{A}\beta_{\text{o}}$ -mediated synaptic dysfunction. Further upstream in the signaling pathway, we implicate Ca^{2+} entry via $\text{Ca}_{\text{v}}2.3$, itself opened by ENaC-mediated depolarization, in the activation of PKC, which then phosphorylates and negatively regulates GSK-3 β . The distinct molecular properties of $\text{Ca}_{\text{v}}2.3$, which opens at significantly more negative potentials than the principal presynaptic VGCC subtypes $\text{Ca}_{\text{v}}2.1$ and $\text{Ca}_{\text{v}}2.2$, suggest that it may be particularly amenable to activation by modest, subthreshold depolarization²³ such as that mediated via ENaCs at the presynaptic terminal.²¹ Presynaptic $\text{Ca}_{\text{v}}2.3$ has previously been

implicated mainly as a trigger of spontaneous neurotransmitter release, a role that also exploits its greater probability of opening at close to resting membrane potential.⁵⁶ Here, however, its special properties allow it to function in the novel context of an intracellular signal transduction pathway, where it serves to link subthreshold membrane depolarization to the upregulation of kinase activity.

In summary, our data demonstrate a critical role for enhanced $\text{Ca}_v2.1$ activity in $\text{A}\beta_0$ -mediated presynaptic dysfunction. Furthermore, they identify $\text{Ca}_v2.1$, together with components of the signaling pathway linking $\text{A}\beta_0$ s to $\text{Ca}_v2.1$, as a potential target that may merit further investigation for therapeutic approaches aimed at mitigating the toxicity of $\text{A}\beta_0$ s at either the synapse or the network level via the normalization of presynaptic function.

Limitations of the study

This study has some technical limitations. The neuronal culture work, as well as some of the acute slice work, is reliant on the use of a variety of pharmacological inhibitors of protein function. While these are valuable tools, pharmacological agents are less specific than genetic interventions and come with off-target effects of varying severity and significance. While the agents used in our study have relatively high target specificity, particularly the peptides such as the $\text{Ca}_v2.1$ blocker ω -agatoxin IVA, contamination of responses by off-target effects is always a possibility. In our case, we have attempted to mitigate this as much as possible by using these drugs for as short a duration, and at as low a concentration, as possible. We have also supported each pharmacological experiment with at least one orthogonal line of evidence using a non-pharmacological approach. A further potential limitation of the study relates to the use of an hAPP transgenic mouse model. While these mice represent the most pathophysiological intact model available for an interventional study of this kind, they do not represent a complete model of the human AD brain, since they lack key features, including the presence of pathological tau deposits and, perhaps most importantly, the many and varied effects of decades of brain aging on which the disease process is usually superimposed. In studies using these mice, it is therefore highly desirable to obtain some evidence from human AD brain tissue in support of the main conclusions, as we have done here.

RESOURCE AVAILABILITY

Lead contact

Requests for further information and resources and reagents should be directed to and will be fulfilled by the lead contact, Alexander Jeans (alexander.jeans@pharm.ox.ac.uk).

Materials availability

This study did not generate new unique reagents.

Data code and availability

- All data supporting the findings of this study are available either within the paper or from the [lead contact](#) upon request.
- This paper does not report original code.
- Any additional information required to reanalyze the data reported in this paper is available from the [lead contact](#) upon request.

ACKNOWLEDGMENTS

We thank Leon Lagnado and Yongling Zhu for gifts of plasmids and the members of the Emptage laboratory for comments on the manuscript. This work was supported by an MRC (UK) Clinician Scientist Fellowship (G0802812) and Centenary Award to A.F.J.

AUTHOR CONTRIBUTIONS

A.F.J. designed experiments, performed experiments, analyzed data, and wrote the paper. Z.P., H.C., W.F., S.A., and S.D. performed experiments and analyzed data. W.L.K. characterized and contributed $\text{A}\beta_0$ preparations. A.M.J.M.v.d.M. contributed the *Cacna1a*-knockout mouse line. N.J.E. provided oversight for the work. All authors revised the manuscript.

DECLARATION OF INTERESTS

The authors declare no competing interests.

STAR★METHODS

Detailed methods are provided in the online version of this paper and include the following:

- [KEY RESOURCES TABLE](#)
- [EXPERIMENTAL MODEL AND STUDY PARTICIPANT DETAILS](#)
 - Animal models
 - Primary cultures
- [METHOD DETAILS](#)
 - Preparation, characterization and use of $\text{A}\beta$ oligomers
 - Adenoviral infection and plasmid transfections
 - Patch-clamp electrophysiology in cultured hippocampal neurons
 - Live cell imaging and analysis
 - Optical fluctuation analysis
 - Immunofluorescence and quantification
 - Protein kinase C activity assay
 - Preparation of acute hippocampal slices and slice electrophysiology
 - FM dye loading and unloading in acute hippocampal slices
 - Human tissue
 - Co-immunoprecipitation
 - Western blotting
- [QUANTIFICATION AND STATISTICAL ANALYSIS](#)

SUPPLEMENTAL INFORMATION

Supplemental information can be found online at <https://doi.org/10.1016/j.celrep.2025.115451>.

Received: July 9, 2024

Revised: February 6, 2025

Accepted: February 28, 2025

Published: March 23, 2025

REFERENCES

1. Mucke, L., and Selkoe, D.J. (2012). Neurotoxicity of amyloid beta-protein: synaptic and network dysfunction. *Cold Spring Harb. Perspect. Med.* 2, a006338. <https://doi.org/10.1101/cshperspect.a006338>.
2. De Strooper, B., and Karvan, E. (2016). The Cellular Phase of Alzheimer's Disease. *Cell* 164, 603–615. <https://doi.org/10.1016/j.cell.2015.12.056>.
3. Busche, M.A., and Konnerth, A. (2016). Impairments of neural circuit function in Alzheimer's disease. *Philos. Trans. R. Soc. Lond. B Biol. Sci.* 371, 20150429. <https://doi.org/10.1098/rstb.2015.0429>.
4. Verret, L., Mann, E.O., Hang, G.B., Barth, A.M.I., Cobos, I., Ho, K., Devidze, N., Masliah, E., Kreitzer, A.C., Mody, I., et al. (2012). Inhibitory

interneuron deficit links altered network activity and cognitive dysfunction in Alzheimer model. *Cell* 149, 708–721. <https://doi.org/10.1016/j.cell.2012.02.046>.

5. Zott, B., Simon, M.M., Hong, W., Unger, F., Chen-Engerer, H.J., Frosch, M.P., Sakmann, B., Walsh, D.M., and Konnerth, A. (2019). A vicious cycle of beta amyloid-dependent neuronal hyperactivation. *Science* 365, 559–565. <https://doi.org/10.1126/science.aa0198>.
6. Cline, E.N., Bicca, M.A., Viola, K.L., and Klein, W.L. (2018). The Amyloid-beta Oligomer Hypothesis: Beginning of the Third Decade. *J. Alzheimers Dis.* 64, S567–s610. <https://doi.org/10.3233/JAD-179941>.
7. Lambert, M.P., Barlow, A.K., Chromy, B.A., Edwards, C., Freed, R., Liosatos, M., Morgan, T.E., Rozovsky, I., Trommer, B., Viola, K.L., et al. (1998). Diffusible, nonfibrillar ligands derived from Abeta1-42 are potent central nervous system neurotoxins. *Proc. Natl. Acad. Sci. USA* 95, 6448–6453.
8. Shankar, G.M., Li, S., Mehta, T.H., Garcia-Munoz, A., Shepardson, N.E., Smith, I., Brett, F.M., Farrell, M.A., Rowan, M.J., Lemere, C.A., et al. (2008). Amyloid-beta protein dimers isolated directly from Alzheimer's brains impair synaptic plasticity and memory. *Nat. Med.* 14, 837–842. <https://doi.org/10.1038/nm1782>.
9. Granseth, B., Odermatt, B., Royle, S.J., and Lagnado, L. (2006). Clathrin-mediated endocytosis is the dominant mechanism of vesicle retrieval at hippocampal synapses. *Neuron* 51, 773–786. <https://doi.org/10.1016/j.neuron.2006.08.029>.
10. Bae, J.R., Lee, W., Jo, Y.O., Han, S., Koh, S., Song, W.K., and Kim, S.H. (2020). Distinct synaptic vesicle recycling in inhibitory nerve terminals is coordinated by SV2A. *Prog. Neurobiol.* 194, 101879. <https://doi.org/10.1016/j.pneurobio.2020.101879>.
11. Zhu, Y., Xu, J., and Heinemann, S.F. (2009). Two pathways of synaptic vesicle retrieval revealed by single-vesicle imaging. *Neuron* 61, 397–411. <https://doi.org/10.1016/j.neuron.2008.12.024>.
12. Catterall, W.A., and Few, A.P. (2008). Calcium channel regulation and pre-synaptic plasticity. *Neuron* 59, 882–901. <https://doi.org/10.1016/j.neuron.2008.09.005>.
13. Akerboom, J., Chen, T.W., Wardill, T.J., Tian, L., Marvin, J.S., Mutlu, S., Calderón, N.C., Esposti, F., Borghuis, B.G., Sun, X.R., et al. (2012). Optimization of a GCaMP calcium indicator for neural activity imaging. *J. Neurosci.* 32, 13819–13840. <https://doi.org/10.1523/jneurosci.2601-12.2012>.
14. Sabatini, B.L., and Svoboda, K. (2000). Analysis of calcium channels in single spines using optical fluctuation analysis. *Nature* 408, 589–593. <https://doi.org/10.1038/35046076>.
15. Parekh, A.B. (2008). Ca²⁺ microdomains near plasma membrane Ca²⁺ channels: impact on cell function. *J. Physiol.* 586, 3043–3054. <https://doi.org/10.1113/jphysiol.2008.153460>.
16. Sinha, S.R., Wu, L.G., and Saggau, P. (1997). Presynaptic calcium dynamics and transmitter release evoked by single action potentials at mammalian central synapses. *Biophys. J.* 72, 637–651. [https://doi.org/10.1016/s0006-3495\(97\)78702-2](https://doi.org/10.1016/s0006-3495(97)78702-2).
17. Takahashi, T., and Momiyama, A. (1993). Different types of calcium channels mediate central synaptic transmission. *Nature* 366, 156–158. <https://doi.org/10.1038/366156a0>.
18. Jeans, A.F., van Heusden, F.C., Al-Mubarak, B., Padamsey, Z., and Emptage, N.J. (2017). Homeostatic Presynaptic Plasticity Is Specifically Regulated by P/Q-type Ca(2+) Channels at Mammalian Hippocampal Synapses. *Cell Rep.* 21, 341–350. <https://doi.org/10.1016/j.celrep.2017.09.061>.
19. Turrigiano, G. (2012). Homeostatic synaptic plasticity: local and global mechanisms for stabilizing neuronal function. *Cold Spring Harb. Perspect. Biol.* 4, a005736. <https://doi.org/10.1101/cshperspect.a005736>.
20. Orr, B.O., Hauswirth, A.G., Celona, B., Fetter, R.D., Zunino, G., Kwon, E.Z., Zhu, Y., Pennacchio, L.A., Black, B.L., and Davis, G.W. (2020). Presynaptic Homeostasis Opposes Disease Progression in Mouse Models of ALS-2.
- Like Degeneration: Evidence for Homeostatic Neuroprotection. *Neuron* 107, 95–111.e6. <https://doi.org/10.1016/j.neuron.2020.04.009>.
21. Younger, M.A., Müller, M., Tong, A., Pym, E.C., and Davis, G.W. (2013). A presynaptic ENaC channel drives homeostatic plasticity. *Neuron* 79, 1183–1196. <https://doi.org/10.1016/j.neuron.2013.06.048>.
22. Kleyman, T.R., and Cragoe, E.J., Jr. (1988). Amiloride and its analogs as tools in the study of ion transport. *J. Membr. Biol.* 105, 1–21. <https://doi.org/10.1007/BF01871102>.
23. Li, L., Bischofberger, J., and Jonas, P. (2007). Differential gating and recruitment of P/Q-N and R-type Ca²⁺ channels in hippocampal mossy fiber boutons. *J. Neurosci.* 27, 13420–13429. <https://doi.org/10.1523/JNEUROSCI.1709-07.2007>.
24. Maravall, M., Mainen, Z.F., Sabatini, B.L., and Svoboda, K. (2000). Estimating intracellular calcium concentrations and buffering without wavelength ratioing. *Biophys. J.* 78, 2655–2667. [https://doi.org/10.1016/S0006-3495\(00\)76809-3](https://doi.org/10.1016/S0006-3495(00)76809-3).
25. Tang, A.H., Karson, M.A., Nagode, D.A., McIntosh, J.M., Uebele, V.N., Renger, J.J., Klugmann, M., Milner, T.A., and Alger, B.E. (2011). Nerve terminal nicotinic acetylcholine receptors initiate quantal GABA release from perisomatic interneurons by activating axonal T-type (Cav3) Ca(2)(+) channels and Ca(2)(+) release from stores. *J. Neurosci.* 31, 13546–13561. <https://doi.org/10.1523/JNEUROSCI.2781-11.2011>.
26. He, Y., Wei, M., Wu, Y., Qin, H., Li, W., Ma, X., Cheng, J., Ren, J., Shen, Y., Chen, Z., et al. (2019). Amyloid beta oligomers suppress excitatory transmitter release via presynaptic depletion of phosphatidylinositol-4,5-bisphosphate. *Nat. Commun.* 10, 1193. <https://doi.org/10.1038/s41467-019-09114-z>.
27. Tanaka, C., and Nishizuka, Y. (1994). The protein kinase C family for neuronal signaling. *Annu. Rev. Neurosci.* 17, 551–567. <https://doi.org/10.1146/annurev.ne.17.030194.003003>.
28. Lipstein, N., Göth, M., Piotrowski, C., Pagel, K., Sinz, A., and Jahn, O. (2017). Presynaptic Calmodulin targets: lessons from structural proteomics. *Expert Rev. Proteomics* 14, 223–242. <https://doi.org/10.1080/14789450.2017.1275966>.
29. Gifford, J.L., Walsh, M.P., and Vogel, H.J. (2007). Structures and metal-ion-binding properties of the Ca²⁺-binding helix-loop-helix EF-hand motifs. *Biochem. J.* 405, 199–221. <https://doi.org/10.1042/BJ20070255>.
30. Fioravante, D., Chu, Y., Myoga, M.H., Leitges, M., and Regehr, W.G. (2011). Calcium-dependent isoforms of protein kinase C mediate postsynaptic potentiation at the calyx of Held. *Neuron* 70, 1005–1019. <https://doi.org/10.1016/j.neuron.2011.04.019>.
31. Ermolyuk, Y.S., Alder, F.G., Henneberger, C., Rusakov, D.A., Kullmann, D.M., and Volynski, K.E. (2012). Independent regulation of basal neurotransmitter release efficacy by variable Ca(2)+ influx and bouton size at small central synapses. *PLoS Biol.* 10, e1001396. <https://doi.org/10.1371/journal.pbio.1001396>.
32. Zhu, L.Q., Liu, D., Hu, J., Cheng, J., Wang, S.H., Wang, Q., Wang, F., Chen, J.G., and Wang, J.Z. (2010). GSK-3 beta inhibits presynaptic vesicle exocytosis by phosphorylating P/Q-type calcium channel and interrupting SNARE complex formation. *J. Neurosci.* 30, 3624–3633. <https://doi.org/10.1523/jneurosci.5223-09.2010>.
33. Beurel, E., Grieco, S.F., and Jope, R.S. (2015). Glycogen synthase kinase-3 (GSK3): regulation, actions, and diseases. *Pharmacol. Ther.* 148, 114–131. <https://doi.org/10.1016/j.pharmthera.2014.11.016>.
34. Kumar, P., Lyle, K.S., Gierke, S., Matov, A., Danuser, G., and Wittmann, T. (2009). GSK3beta phosphorylation modulates CLASP-microtubule association and lamella microtubule attachment. *J. Cell Biol.* 184, 895–908. <https://doi.org/10.1083/jcb.200901042>.
35. Li, D., Wang, F., Lai, M., Chen, Y., and Zhang, J.F. (2005). A protein phosphatase 2alpha-Ca²⁺ channel complex for dephosphorylation of neuronal Ca²⁺ channels phosphorylated by protein kinase C. *J. Neurosci.* 25, 1914–1923. <https://doi.org/10.1523/JNEUROSCI.4790-04.2005>.

36. Cheung, T.T., Ismail, N.A.S., Moir, R., Arora, N., McDonald, F.J., and Condilffe, S.B. (2019). Annexin II Light Chain p11 Interacts With ENaC to Increase Functional Activity at the Membrane. *Front. Physiol.* 10, 7. <https://doi.org/10.3389/fphys.2019.00007>.

37. Dougherty, J.J., Wu, J., and Nichols, R.A. (2003). Beta-amyloid regulation of presynaptic nicotinic receptors in rat hippocampus and neocortex. *J. Neurosci.* 23, 6740–6747.

38. Renner, M., Lacor, P.N., Velasco, P.T., Xu, J., Contractor, A., Klein, W.L., and Triller, A. (2010). Deleterious effects of amyloid beta oligomers acting as an extracellular scaffold for mGluR5. *Neuron* 66, 739–754. <https://doi.org/10.1016/j.neuron.2010.04.029>.

39. Glasgow, S.D., McPhedrain, R., Madranges, J.F., Kennedy, T.E., and Ruthazer, E.S. (2019). Approaches and Limitations in the Investigation of Synaptic Transmission and Plasticity. *Front. Synaptic Neurosci.* 11, 20. <https://doi.org/10.3389/fnsyn.2019.00020>.

40. Li, S., Hong, S., Shepardson, N.E., Walsh, D.M., Shankar, G.M., and Selkoe, D. (2009). Soluble oligomers of amyloid Beta protein facilitate hippocampal long-term depression by disrupting neuronal glutamate uptake. *Neuron* 62, 788–801. <https://doi.org/10.1016/j.neuron.2009.05.012>.

41. Christie, L.A., Russell, T.A., Xu, J., Wood, L., Shepherd, G.M.G., and Contractor, A. (2010). AMPA receptor desensitization mutation results in severe developmental phenotypes and early postnatal lethality. *Proc. Natl. Acad. Sci. USA* 107, 9412–9417. <https://doi.org/10.1073/pnas.0908206107>.

42. Heine, M., Groc, L., Frischknecht, R., Béïque, J.C., Lounis, B., Rumbaugh, G., Huganir, R.L., Cognet, L., and Choquet, D. (2008). Surface mobility of postsynaptic AMPARs tunes synaptic transmission. *Science* 320, 201–205. <https://doi.org/10.1126/science.1152089>.

43. Taylor, H.B.C., Emptage, N.J., and Jeans, A.F. (2021). Long-term depression links amyloid-beta to the pathological hyperphosphorylation of tau. *Cell Rep.* 36, 109638. <https://doi.org/10.1016/j.celrep.2021.109638>.

44. Mucke, L., Masliah, E., Yu, G.Q., Mallory, M., Rockenstein, E.M., Tatsuno, G., Hu, K., Kholodenko, D., Johnson-Wood, K., and McConlogue, L. (2000). High-level neuronal expression of abeta 1-42 in wild-type human amyloid protein precursor transgenic mice: synaptotoxicity without plaque formation. *J. Neurosci.* 20, 4050–4058.

45. Kavalali, E.T., and Jorgensen, E.M. (2014). Visualizing presynaptic function. *Nat. Neurosci.* 17, 10–16. <https://doi.org/10.1038/nn.3578>.

46. Kaja, S., van de Ven, R.C.G., Broos, L.A.M., Frants, R.R., Ferrari, M.D., van den Maagdenberg, A.M.J.M., and Plomp, J.J. (2007). Characterization of acetylcholine release and the compensatory contribution of non-Ca(v)2.1 channels at motor nerve terminals of leaner Ca(v)2.1-mutant mice. *Neuroscience* 144, 1278–1287. <https://doi.org/10.1016/j.neuroscience.2006.11.006>.

47. Fletcher, C.F., Tottene, A., Lennon, V.A., Wilson, S.M., Dubel, S.J., Paylor, R., Hosford, D.A., Tessarollo, L., McEnery, M.W., Pietrobon, D., et al. (2001). Dystonia and cerebellar atrophy in Cacna1a null mice lacking P/Q calcium channel activity. *FASEB J.* 15, 1288–1290. <https://doi.org/10.1096/fj.00-0562fje>.

48. Masliah, E., Ellisman, M., Carragher, B., Mallory, M., Young, S., Hansen, L., DeTeresa, R., and Terry, R.D. (1992). Three-dimensional analysis of the relationship between synaptic pathology and neuropil threads in Alzheimer disease. *J. Neuropathol. Exp. Neurol.* 51, 404–414. <https://doi.org/10.1097/00005072-199207000-00003>.

49. Bakker, A., Krauss, G.L., Albert, M.S., Speck, C.L., Jones, L.R., Stark, C.E., Yassa, M.A., Bassett, S.S., Shelton, A.L., and Gallagher, M. (2012). Reduction of hippocampal hyperactivity improves cognition in amnestic mild cognitive impairment. *Neuron* 74, 467–474. <https://doi.org/10.1016/j.neuron.2012.03.023>.

50. Sarter, M., Bruno, J.P., and Parikh, V. (2007). Abnormal neurotransmitter release underlying behavioral and cognitive disorders: toward concepts of dynamic and function-specific dysregulation. *Neuropsychopharmacology* 32, 1452–1461. <https://doi.org/10.1038/sj.npp.1301285>.

51. Brito-Moreira, J., Paula-Lima, A.C., Bomfim, T.R., Oliveira, F.B., Sepulveda, F.J., De Mello, F.G., Aguayo, L.G., Panizzutti, R., and Ferreira, S.T. (2011). Abeta oligomers induce glutamate release from hippocampal neurons. *Curr. Alzheimer Res.* 8, 552–562.

52. Nimmrich, V., Grimm, C., Draguhn, A., Barghorn, S., Lehmann, A., Schoemaker, H., Hillen, H., Gross, G., Ebert, U., and Bruehl, C. (2008). Amyloid beta oligomers (A beta(1-42) globulomer) suppress spontaneous synaptic activity by inhibition of P/Q-type calcium currents. *J. Neurosci.* 28, 788–797. <https://doi.org/10.1523/jneurosci.4771-07.2008>.

53. Parodi, J., Sepulveda, F.J., Roa, J., Opazo, C., Inestrosa, N.C., and Aguayo, L.G. (2010). Beta-amyloid causes depletion of synaptic vesicles leading to neurotransmission failure. *J. Biol. Chem.* 285, 2506–2514. <https://doi.org/10.1074/jbc.M109.030023>.

54. Russell, C.L., Semerdjeva, S., Empson, R.M., Austen, B.M., Beesley, P.W., and Alifragis, P. (2012). Amyloid-beta acts as a regulator of neurotransmitter release disrupting the interaction between synaptophysin and VAMP2. *PLoS One* 7, e43201. <https://doi.org/10.1371/journal.pone.0043201>.

55. Palop, J.J., Chin, J., Roberson, E.D., Wang, J., Thwin, M.T., Bien-Ly, N., Yoo, J., Ho, K.O., Yu, G.Q., Kreitzer, A., et al. (2007). Aberrant excitatory neuronal activity and compensatory remodeling of inhibitory hippocampal circuits in mouse models of Alzheimer's disease. *Neuron* 55, 697–711. <https://doi.org/10.1016/j.neuron.2007.07.025>.

56. Ermolyuk, Y.S., Alder, F.G., Surges, R., Pavlov, I.Y., Timofeeva, Y., Kullmann, D.M., and Volynski, K.E. (2013). Differential triggering of spontaneous glutamate release by P/Q-N- and R-type Ca²⁺ channels. *Nat. Neurosci.* 16, 1754–1763. <https://doi.org/10.1038/nn.3563>.

57. Jankowsky, J.L., Slunt, H.H., Gonzales, V., Savonenko, A.V., Wen, J.C., Jenkins, N.A., Copeland, N.G., Younkin, L.H., Lester, H.A., Younkin, S.G., and Borchelt, D.R. (2005). Persistent amyloidosis following suppression of Abeta production in a transgenic model of Alzheimer disease. *PLoS Med.* 2, e355. <https://doi.org/10.1371/journal.pmed.0020355>.

58. Klein, W.L. (2002). Abeta toxicity in Alzheimer's disease: globular oligomers (ADDLs) as new vaccine and drug targets. *Neurochem. Int.* 41, 345–352.

59. Peng, C., Yan, Y., Kim, V.J., Engle, S.E., Berry, J.N., McIntosh, J.M., Neve, R.L., and Drenan, R.M. (2019). Gene editing vectors for studying nicotinic acetylcholine receptors in cholinergic transmission. *Eur. J. Neurosci.* 50, 2224–2238. <https://doi.org/10.1111/ejn.13957>.

60. Padamsey, Z., McGuinness, L., Bardo, S.J., Reinhart, M., Tong, R., Hedegaard, A., Hart, M.L., and Emptage, N.J. (2017). Activity-Dependent Exocytosis of Lysosomes Regulates the Structural Plasticity of Dendritic Spines. *Neuron* 93, 132–146. <https://doi.org/10.1016/j.neuron.2016.11.013>.

61. Schwarz, G. (1978). Estimating the Dimension of a Model. *Ann. Statist.* 6, 461–464.

STAR★METHODS

KEY RESOURCES TABLE

REAGENT or RESOURCE	SOURCE	IDENTIFIER
Antibodies		
Guinea pig polyclonal anti-synaptophysin	Synaptic Systems	Cat# 101 004; RRID AB_1210382
Mouse monoclonal anti-GSK-3 β	Cell Signaling Technology	Cat# 9832; RRID AB_10839406
Rabbit polyclonal anti-phospho-GSK-3 β (S9)	St. John's Laboratory	Cat# STJ22160
Rabbit polyclonal anti-ENaC α -subunit	StressMarq	Cat# SPC-403; RRID AB_10640131
Goat polyclonal anti-guinea pig AlexaFluor 405-conjugated	Abcam	Cat# ab175678; RRID AB_2827755
Goat polyclonal anti-mouse AlexaFluor 488-conjugated	Abcam	Cat# ab150117; RRID AB_2688012
Goat polyclonal anti-rabbit AlexaFluor 594-conjugated	Abcam	Cat# ab150080; RRID AB_2650602
Rabbit polyclonal anti-CACNA1A (Ca V 2.1)	Alomone Labs	Cat# ACC-001; RRID AB_2039764
Mouse monoclonal anti-syntaxin 1	Synaptic Systems	Cat# 110 011; RRID AB_887844
Goat polyclonal anti-mouse IRDye 800CW-conjugated	Li-Cor Biosciences	P/N 926-32210; RRID AB_621842
Donkey polyclonal anti-rabbit IRDye 680LT-conjugated	Li-Cor Biosciences	P/N 926-68023; RRID AB_10706167
Bacterial and virus strains		
Adenovirus Ad-SyPhyA4	Vector Biolabs	N/A
Biological samples		
Alzheimer's disease and control BA9 brain tissue	London Neurodegenerative Diseases Brain Bank (https://www.kcl.ac.uk/neuroscience/facilities/brain-bank)	N/A
Chemicals, peptides, and recombinant proteins		
Lipofectamine 2000	Thermo Fisher Scientific	Cat# 11668027
$\text{A}\beta_{1-42}$ peptide	Abcam	Cat# ab82795
NBQX	Abcam	Cat# ab144489
D-AP5 (APV)	Abcam	Cat# ab120003
ω -Agatoxin IVA	Alomone Labs	Cat# STA-500
ω -Conotoxin GVIA	Alomone Labs	Cat# C-300
Amiloride	Sigma-Aldrich	Cat# A7410
BAPTA	Thermo Fisher Scientific	Cat# B1204
SNX-482	Alomone Labs	Cat# RTS-500
SIB-1757	Tocris	Cat# 1215
Go 6976	Abcam	Cat# ab141413
Tautomycin	Sigma-Aldrich	Cat# 580551
α -Bungarotoxin	Sigma-Aldrich	Cat# 203980
Ionomycin	Thermo Fisher Scientific	Cat# I24222
Syn-PER	Thermo Fisher Scientific	Cat# 87793
TAMRA-conjugated $\text{A}\beta_{1-42}$	AnaSpec	Cat# ANA60476
α -Bungarotoxin CF594	Biotium	Cat# BT00007
Cyclothiazide	Abcam	Cat# ab120323
FM1-43	Thermo Fisher Scientific	Cat# T3163
ADVASEP-7	Biotium	Cat# BT70029

(Continued on next page)

Continued

REAGENT or RESOURCE	SOURCE	IDENTIFIER
Critical commercial assays		
Bradford Plus Protein Assay	Thermo Fisher Scientific	Cat# 23238
PKC kinase activity kit	Enzo Life Sciences	Cat# ADI-EKS-420A
Experimental models: Organisms/strains		
Wistar rats	Charles River Laboratories UK	Strain code 003; RRID RGD_737929
C57BL/6J mice	Oxford University Biomedical Services	RRID IMSR_JAX:000664
B6.Cg-Zbtb20 ^{Tg(PDGFB-APPSwInd)20Lms/2Mmjax} (J20)	Mucke et al. ⁴⁴	https://www.jax.org/strain/006293#
Cacna1a knockout mice	Kaja et al. ⁴⁶	N/A
B6.Cg-Tg(tetO-APPSwInd)102Dbo/Mmjjax	Jankowsky et al. ⁵⁷	https://www.jax.org/strain/007051
Recombinant DNA		
Plasmid SypHy	Granseth et al. ⁹	Addgene plasmid# 24478
Plasmid SypH 2x	Zhu et al. ¹¹	Addgene plasmid# 37004
Plasmid SyGCamP5	Akerboom et al. ¹³	N/A
Plasmid GAD67 ^{pro} -vGAT-pH	Bae et al. ¹⁰	N/A
Plasmid sgRNA <i>Chrna7</i> (g13)	This paper	N/A
Plasmid sgRNA luciferase	This paper	N/A
Software and algorithms		
iQ	Andor	https://andor.oxinst.com/products/ ; RRID SCR_014461
ImageJ	NIH	https://imagej.nih.gov/ij/ ; RRID SCR_003070
WinWCP	Strathclyde University	https://spider.science.strath.ac.uk/sipbs/software_ses.htm ; RRID SCR_014713
Li-Cor Image Studio Lite	Li-Cor Biosciences	https://www.licor.com/bio/image-studio-lite/ ; RRID SCR_013715
MATLAB	MathWorks	https://www.mathworks.com/products/matlab.html ; RRID SCR_001622
Prism	GraphPad	https://www.graphpad.com/scientific-software/prism/ ; RRID SCR_002798

EXPERIMENTAL MODEL AND STUDY PARTICIPANT DETAILS

Animal models

All mouse work was carried out in accordance with the Animals (Scientific Procedures) Act, 1986 (UK) and under project and personal licenses approved by the Home Office (UK). Both the *Cacna1a* knockout (from Prof. A. van den Maagdenberg, Leiden University Medical Centre) and J20 hAPP transgenic (kind gift of Prof. D. Anthony, University of Oxford) mouse lines were on a C57BL/6J background, and the lines were maintained by crossing heterozygotes or hemizygotes with wild-type C57BL/6J mice. Crossing hAPP hemizygote with *Cacna1a*^{+/+} mice yielded all four of the genotypes used in the FM dye assays, and animals used in these experiments were therefore littermates. For co-immunoprecipitation experiments only, another mouse line carrying, like J20, an APP transgene with Swedish and Indiana mutations, was used. Line B6.Cg-Tg(tetO-APPSwInd)102Dbo/Mmjjax was crossed with a CamKIIα-tTA line to activate hAPP expression,⁵⁷ and 20 month old double transgenic (tTA/hAPP) individuals along with accompanying non-transgenic littermate controls, a kind gift of Dr. Mariana Vargas-Caballero, were used. Mice were housed in group cages in a facility with controlled temperature and lighting (alternating 12 hour light/dark cycles). All genotyping was carried out by Transnetyx Inc. Mice of both sexes were used in all experiments.

Primary cultures

Dissociated hippocampal cultures were prepared from E18 Wistar rat embryos of both sexes as already described.¹⁸ Briefly, hippocampal neurons were seeded onto poly-D-lysine-coated coverslips and cultured in Neurobasal medium supplemented with 2% fetal calf serum (FCS), 2% B27, 1% Glutamax and 1% penicillin/streptomycin. The day after plating, half the medium was changed for Neurobasal supplemented with 2% B27 and 1% Glutamax only; this medium was used for all further feeds. Cultures were maintained in a humidified incubator at 37°C with 5% CO₂.

METHOD DETAILS**Preparation, characterization and use of A β oligomers**

Oligomers were prepared from A β ₁₋₄₂ peptide as previously described.⁵⁸ Briefly, solid A β ₁₋₄₂ was dissolved in cold hexafluoro-2-propanol (HFIP; Sigma-Aldrich). The peptide was incubated at room temperature for at least 1 hour to establish monomerization and randomization of structure. The HFIP was aliquoted and allowed to evaporate overnight, followed by 10 minutes in a Savant Speed Vac. The resulting peptide was stored as a film at -80 °C. The film was dissolved in anhydrous dimethylsulfoxide (Sigma-Aldrich) to 5 mM, diluted to 100 μ M with Ham's F12 (without phenol red, with glutamine; Caisson Laboratories) and briefly vortexed. The solution was incubated at 4 °C for 22-24 hours and soluble oligomers obtained by centrifugation at 14,000 g for 10 minutes at 4 °C. Protein concentration was estimated using the Bradford Plus Protein Assay and a bovine serum albumin (BSA) standard. For shipping purposes, small aliquots of the soluble oligomers were dried using a Savant Speed Vac and reconstituted with cold sterile water and gentle pipetting immediately prior to use. Tetramethyl rhodamine (TAMRA)-conjugated A β ₁₋₄₂ was subjected to the same protocol to prepare fluorescently-tagged oligomers.

Adenoviral infection and plasmid transfections

SyPhy (kind gift of Prof. L. Lagnado) was cloned into an adenoviral expression vector using the Ad-HQ system, and packaged to produce an active human Adenovirus Type 5 (dE1/E3). This was used to infect cultured hippocampal neurons 8 days after plating at a multiplicity of infection (MOI) of 0.2. All other plasmids were introduced into neurons 8 days after plating using Lipofectamine 2000. For each well, DNA and Lipofectamine were added to 200 μ L Neurobasal at a ratio of 3 μ g:3 μ L and incubated for 20 minutes before transfection, which was carried out in 2 mL of medium per well. Transfection mix was incubated with the cultures for 1 hour before being removed and replaced with a 2:1 ratio of conditioned to fresh medium. The SyPhy 2x plasmid was a gift of Dr. Y. Zhu, the GAD67^{pro}-vGAT-pH plasmid was a gift of Prof. S. H. Kim and SyGCamp5 was a gift of Prof. L. Lagnado. The CRISPR/Cas9 plasmids were generated by the Weatherall Institute of Molecular Medicine Genome Engineering Facility (University of Oxford) and based on the vector px458 into which sequences coding for sgRNA directed against either the firefly luciferase gene (control) or mouse *Chrna7* (g13)⁵⁹ were cloned.

Patch-clamp electrophysiology in cultured hippocampal neurons

Whole-cell patch recordings were made using either an Axoclamp 900A or an Axoscope 2B amplifier (both Axon Instruments). Data was low-pass filtered at 3k Hz, sampled at >10kHz. Data was acquired using WinWCP and analyzed using Clampfit software. Patch electrodes (4-8 M Ω) contained (in mM): 120 CsMeSO₄, 10 KCl, 10 NaPhosphocreatine, 10 HEPES, 4 MgATP and 0.4 Na₃GTP. Spontaneous activity was recorded in Tyrode's solution containing (in mM): 120 NaCl, 30 Glucose, 25 HEPES, 5.4 KCl, 1.5 CaCl₂ and 0.5 MgCl₂.

Live cell imaging and analysis

Experiments were performed 14-21 days after plating (6-13 days after transfection) when synapses are mature. Coverslips were mounted in a Chamlide EC-B18 stimulation chamber (Live Cell Instrument) on the stage of an Olympus IX-71 inverted microscope fitted with a 100X, NA 1.40 UPlanSApo objective and an Andor iXon EM CCD camera, and stimulation and imaging of live neurons was carried out as described.¹⁸ Phluorin imaging was carried out at 1 Hz for 100 AP stimulation and 5 Hz for 1 AP stimulation; Ca²⁺ imaging was carried out at 10 Hz. All time series images were acquired with 2 X 2 pixel binning. Unless otherwise specified, A β ₀ were applied at 200 nM (monomer equivalent) in culture medium in the incubator for 2 hours. Where cells had been incubated with A β ₀ or vehicle, these were present throughout the experiment. Where the following were used they were added 10 minutes before A β ₀ or vehicle treatment and were present throughout the incubation and experiment: ω -Agatoxin IVA (100 nM); ω -conotoxin GVIA (250 nM); amiloride (100 μ M); BAPTA (5 mM tetrapotassium salt); SNX-482 (500 nM); SIB-1757 (3 μ M); Go 6976 (100 nM); tautomycin (2 nM); α -bungarotoxin (100 nM). In experiments measuring basal Ca²⁺ concentration, ionomycin was used at 10 μ M following initial image acquisition to elicit maximal Ca²⁺ entry; the maximal signal value obtained is used to normalize the basal Ca²⁺ signal measurements to account for differences in SyGCamp5 expression. In experiments imaging binding of either α -bungarotoxin CF594 (100 nM) or TAMRA-conjugated A β ₀ (200 nM), which were applied in the incubator for 10 minutes or 2 hours respectively, the image acquisition system described above was used but with a 900 ms exposure time and no pixel binning.

Time series images were analyzed in ImageJ (<http://rsb.info.nih.gov/ij>) using the Time Series Analyzer plugin (<http://rsb.info.nih.gov/ij/plugins/time-series.html>). All visible varicosities were selected for analysis with a 2 μ m diameter ROI. Terminals were excluded from analysis in pHluorin experiments if their maximum response to 40 AP or 100 AP was less than 2 SD of baseline noise; for Ca²⁺ experiments, terminals were excluded if their peak response to 1 AP averaged over 5 trials was less than 2 SD of baseline noise, or if they did not show a response to ionomycin application. Data exported from ImageJ were background adjusted and pHluorin data were normalized to the peak signal obtained following NH₄Cl application (mean value of plateau over 5 seconds). Ca²⁺ indicator data were normalized to either the basal, unstimulated signal or to the signal elicited by ionomycin. Peak fluorescence in all experiments was taken at the end of the stimulation period. For analysis of single images generated during A β ₀ binding experiments, segmentation was first carried out using inbuilt ImageJ functionality to generate a mask from a 50 μ m section of axon or dendrite in the

GFP channel, and this was then used to measure mean fluorescence in the red fluorophore channel with additional background adjustment. All analysis was performed using custom-written macros or scripts in Microsoft Excel or MATLAB.

Optical fluctuation analysis

Optical fluctuation analysis analyses trial-to-trial variation in Ca^{2+} transients through VGCC to determine whether changes in Ca^{2+} influx are due to changes in the number (N), open probability (p) or unitary channel currents (q) of functional channels.¹⁴ We used the experimentally derived inverse squared coefficient of variation (CV^2) of boutonal Ca^{2+} transients along with a published value for p at cultured hippocampal terminals,⁵⁶ as unfortunately this parameter cannot be experimentally measured, to calculate the mean N at each terminal under control conditions (N = 19.5). We then extrapolated both N and p to values expected if the experimentally observed increase in mean Ca^{2+} transient size following $\text{A}\beta_o$ treatment were solely a result of an increase in either of these parameters alone, and used these to calculate the CV^2 that would be expected after $\text{A}\beta_o$ treatment in each instance. Note that in optical fluctuation analysis, changes in N or p (or some combination of these) are associated with a change in CV^2 , while changes in q are not.

Immunofluorescence and quantification

Cultured neurons were subjected to relevant treatments before being washed twice with PBS; where used, $\text{A}\beta_o$ were applied at 200 nM for 2 hours. The cells were then fixed in 4% paraformaldehyde for 15 minutes on ice. For all experiments except surface ENaC staining, coverslips were then treated with 0.1% saponin or Triton X-100 on ice for 15 minutes, before incubation in 10% FCS in PBS at room temperature for 30 minutes. Cells were then incubated with anti-synaptophysin antibody (1:1000) together with either anti-GSK-3 β (1:1000) and anti-phospho-GSK-3 β (S9) (1:500), or anti-ENaC α -subunit (1:1000). For surface ENaC staining, the procedure was identical except that the primary antibody incubations were carried out in succession, anti-ENaC antibody first, and the permeabilization step, if included, was carried out between the two. Following primary antibody incubation, coverslips were washed, incubated for 1 hour at room temperature with various AlexaFluor-conjugated secondary antibodies, all used at 1 in 400 dilution, washed again and mounted using ProLong Gold antifade (Thermo Fisher Scientific).

Images were collected using an Olympus Fluoview FV1000 confocal system with an Olympus IX-81 inverted microscope, and either a 100X, NA 1.40 UPlanSApo or a 60X, NA 1.35 UPlanSApo oil immersion objective. Images were acquired in Olympus Fluoview software and analyzed using ImageJ as described in the main text or caption. Image segmentation was carried out using inbuilt ImageJ functionality to generate a mask from the synaptophysin channel, and this was then used to measure mean fluorescence in other fluorophore channels as required. For all experiments, image acquisition parameters, as well as any image thresholding applied, were fixed within an experiment to allow for comparison between conditions.

Protein kinase C activity assay

Synaptosomes were prepared 14 days after plating from individual 35 mm culture wells of hippocampal neurons cultured as described above. Syn-PER reagent was used according to the manufacturer's instructions, and each pellet representing synaptosomes from a single well was resuspended in 100 μl Syn-PER, before this was then divided into three parts that were exposed to either a vehicle, $\text{A}\beta_o$ (200 nM) or $\text{A}\beta_o$ + SNX-482 (500 nM) treatment for 2 hours before immediate freezing at -80 °C. Protein concentration in each sample was assessed with a BCA assay, and PKC activity in the samples was then assessed with an ELISA-based kit used according to manufacturer's instructions. Based on preliminary experiments with a purified PKC standard included with the kit, a 0.1 μg total protein equivalent of each sample was loaded per assay well, as this amount gave results within the dynamic range of the assay, and all samples were assayed in duplicate.

Preparation of acute hippocampal slices and slice electrophysiology

Field excitatory postsynaptic potentials (fEPSPs) were recorded in 300 μm thick acute hippocampal slices prepared as described⁶⁰ from 7 to 8 week old C57BL/6J mice, or from aged, genotyped mice as specified. Slices were placed in an interface recording chamber perfused with oxygenated ACSF (2 mM Ca^{2+} , 1 mM Mg^{2+}) at 1 to 2 mL/min, and a bipolar stimulating electrode (FHC Inc., Bowdoin, ME, USA) was placed in Schaffer collaterals to deliver test and conditioning stimuli. For most experiments, a borosilicate glass recording electrode filled with artificial cerebrospinal fluid was positioned in stratum radiatum of CA1. Test responses to stimuli delivered at 0.067 Hz were recorded for at least 10 minutes prior to beginning experiments to ensure stable responses. Field potentials were amplified using a Digitimer NeuroLog amplifier, filtered below 3 Hz and above 3 KHz and digitized with a BNC-2090A converter (National Instruments). Recording was carried out on WinWCP software and analyzed using the Clampfit program. Unless otherwise stated, slices were incubated in drug treatments for > 2 hours prior to the experiment and the drugs were maintained in the perfusing ACSF for the duration of the recording. Concentrations used in all experiments were as follows: ω -agatoxin IVA 400 nM; $\text{A}\beta$ oligomers 10 nM; cyclothiazide 100 μM . Other than these, drugs were not included in the experiments in order to preserve intact neuronal circuits. The magnitude of fEPSPs was determined as the gradient of the rising slope to avoid population spike contamination. Paired-pulse ratios were obtained by delivering two stimuli at intervals as specified and expressed as fEPSP2/fEPSP1.

FM dye loading and unloading in acute hippocampal slices

Slices of 300 μm thickness prepared as above were transferred to a custom-made recording chamber mounted on an Olympus BX50WI microscope fitted with a BioRad Radiance 2000 confocal scanhead (BioRad/Zeiss) and were superfused at 35°C with

oxygenated ACSF (2 mM Ca²⁺, 1 mM Mg²⁺) supplemented with 10 µM NBQX and 50 µM APV to block recurrent activity. A patch pipette was filled with a 20 µM solution of the styryl dye FM1-43 in ACSF and placed in stratum radiatum of CA1 at a depth of approximately 100 µm. The dye was pressure applied for 3 minutes using a custom-made picospritzer before a 10 Hz train of 1200 stimuli (100 µA) was delivered to Schaffer collaterals using a glass stimulating electrode (4-8 MΩ) filled with 150 mM NaCl placed within 70 µm of the dye-filled pipette; the stimulating electrode was under the control of WIN WCP software and a DS3 stimulation box (Digitimer). Pressure application of dye was maintained throughout the loading stimulus and for 2 minutes afterwards to ensure completion of endocytosis. Slices were then perfused continuously in fresh ACSF containing 0.2 mM ADVASEP-7 for 15-20 minutes to wash residual FM dye from extracellular membranes. Imaging of labeled terminals was performed using a 60X, NA 1.1 LUMFL N objective (Olympus), a 488 nm Argon laser for excitation and a 500 nm long-pass emission filter. Image stacks were acquired every 15 seconds throughout the unloading stimulus (3000 stimuli at 10 Hz). Each image stack comprised 6 images of 512 x 512 pixels acquired at 1 µm intervals in the z-axis, and a digital zoom of 3X and 2X Kalman averaging were applied. Images were acquired using Zeiss LaserSharp software and analyzed using ImageJ and custom-written scripts in MATLAB.

Human tissue

Samples of human frontal cortex (Brodmann area 9) were obtained from the MRC London Neurodegenerative Diseases Brain Bank, King's College, London (part of the Brains for Dementia Research initiative) with full ethical approval; 5 AD cases, all BrainNet Europe stage VI or modified Braak stage VI, and 5 age-matched controls, all BrainNet Europe or Braak stage I or II, were used (see [Table S1](#)).

Co-immunoprecipitation

For co-immunoprecipitations, approximately 500 mg of either human or mouse brain tissue was homogenized using a Dounce tissue grinder into 2 mL buffer A containing (in mM): 320 sucrose, 5 Tris base, pH 7.4, 2 EDTA, on ice; note that all buffers used throughout the immunoprecipitations included HALT protease and phosphatase inhibitor cocktail (Thermo Fisher Scientific) at 1:100. After a 10 minute centrifugation at 750 rpm, the supernatant was removed and centrifuged at 17,000 rpm for 1 hour. This yielded a membrane pellet which was resuspended in 1 mL buffer A + 1% CHAPS, and 300 µL of this was rotated for 3 hours at 4°C with Novex magnetic Protein G Dynabeads (Life Technologies) to which anti-Cav2.1 or antibody had previously been bound (see below). After incubation, the beads were retrieved by magnetic separation and washed twice in buffer B containing (in mM): 150 NaCl, 25 Tris base, pH 7.4, 2 EDTA, to which 0.5% BSA and 0.4% CHAPS had also been added. Beads were then washed once in buffer B alone before being resuspended in 100 µL 2X Laemmli sample buffer with 5% β-mercaptoethanol for Western blotting. For binding of antibodies to Protein G Dynabeads, the supplied buffer was removed from 50 µL of bead suspension, and beads were washed once in buffer A + 0.5% BSA + 0.4% CHAPS. 5 µL of anti-Cav2.1 antibody (as used for Western blotting) was then added, and the bead/antibody mixture was rotated for 10 minutes at room temperature before beads were washed twice in buffer A + 0.5% BSA.

Western blotting

Samples were dissolved in 2X Laemmli sample buffer with 5% β-mercaptoethanol, heated to 60°C for 3 minutes and run on a precast 4-20% gradient SDS-PAGE gel (Thermo Fisher Scientific). The separated samples were transferred to a nitrocellulose membrane (Bio-Rad) before blocking with 5% milk and 1% horse serum in TBS with 0.05% Tween-20 (TBST) and subsequent probing with a mixture of anti-Cav2.1 (1:200) and anti-stx1 (1:1000) antibodies. After three TBST washes, bound antibodies were detected with IRDye 680LT donkey anti rabbit IgG (1:20,000) and IRDye 800CW goat anti-mouse IgG (1:15,000) fluorescent secondary antibodies, washed three times in TBST and imaged on a Li-Cor Odyssey system. Image analysis was performed in Li-Cor Image Studio Lite software.

QUANTIFICATION AND STATISTICAL ANALYSIS

Statistical analysis was performed using GraphPad Prism software. Data were assessed for normality using the Shapiro-Wilk test, and analyzed using parametric or non-parametric tests accordingly. Unless otherwise stated, the two-tailed unpaired Student's t test was used to determine the statistical significance of observed differences between various conditions. Where other tests were used, this is clearly stated in the caption of the appropriate figure. Figure captions also contain the details of tests conducted, including n for each test. P values greater than 0.05 were regarded as non-significant. For optical fluctuation analysis, we determined whether changes in N, p or q best described our data using the Bayesian Information Criterion (BIC), with a BIC difference of 10 or more providing strong evidence in favor of the model with the lowest BIC score.⁶¹